STATISTICAL OPTIMIZATION AND MECHANISTIC INSIGHT INTO DYE ADSORPTION USING A NOVEL AC-ZnO-NH$_3$ NANOMATERIAL

AL-SAEEDI, S. I.[1] – ASHOUR, M.[2] – ALPROL, A. E.[3*] – AL-SENANI, G. M.[1]

[1]*Department of Chemistry, College of Science, Princess Nourah bint Abdulrahman University, P.O. Box 84428, Riyadh 11671, Saudi Arabia*

[2]*Fish Resources Research Center, King Faisal University, Hofuf-420, Al-Ahsa 31982, Saudi Arabia*

[3]*National Institute of Oceanography and Fisheries (NIOF), Cairo 11516, Egypt*

**Corresponding author*
e-mail: mashour@kfu.edu.sa

(Received 12th Oct 2025; accepted 6th Jan 2026)

Abstract. This study investigates the efficiency of a zinc oxide and ammonia-modified activated carbon nanocomposite (AC-ZnO-NH$_3$) for removing Acid Red 1 dye from water. Scanning electron microscopy revealed a porous structure with varying particle sizes, while energy-dispersive X-ray analysis confirmed the presence of zinc, iron, oxygen, and carbon. Fourier-transform infrared spectroscopy identified functional groups involved in adsorption, and thermogravimetric analysis demonstrated high thermal stability due to the presence of stable ZnO. The composite exhibited strong antibacterial activity, particularly against *Staphylococcus aureus* and *Streptococcus agalactiae*, suggesting selective efficacy against Gram-positive bacteria. Optimization using the Box-Behnken Design (BBD) under Response Surface Methodology (RSM) indicated that higher pH, longer contact time, greater adsorbent dosage, and lower initial dye concentration enhanced dye removal. The optimal conditions were pH 5, 75 mg/L dye concentration, 0.03 g adsorbent, and 90 min contact time. Kinetic analysis showed that the pseudo-second-order model best described the process, indicating chemical adsorption. The Langmuir isotherm fit the data well, suggesting monolayer adsorption with a capacity of 312.5 mg/g. Thermodynamic results showed the process was endothermic and temperature-dependent. Although adsorption efficiency decreased after one regeneration cycle, the AC-ZnO-NH$_3$ composite demonstrates strong potential as a sustainable material for wastewater decolorization.
Keywords: *Acid Red 1 dye, activated carbon, ammonia, zinc oxide, adsorption, antimicrobial, Box-Behnken design*

Introduction

In the modern world, one of the biggest and most pressing issues facing society and the environment is the process of elimination or reduction of the use of harmful substances (Manisalidis et al., 2020). The discharge of industrial wastewater into aquatic environments represents a pressing global concern, posing significant threats to human health, ecosystem stability, and economic prosperity. Among the diverse range of pollutants released by various industrial processes, synthetic dyes stand out as a major concern due to their persistence, toxicity, and visibility in water bodies (Al-Tohamy et al., 2022). The widespread use of dyes in various industries, including textiles, paper, leather, plastics, and food, results in substantial volumes of dye-laden wastewater being released into the environment (Mansour et al., 2022). Acid Red 1, a prominent azo dye extensively used in textile dyeing, exemplifies the hazards associated with dye pollution. The presence of Acid Red 1 and other toxic dyes in water sources can disrupt delicate

http://www.aloki.hu ● ISSN 1589 1623 (Print) ● ISSN 1785 0037 (Online)
DOI: http://dx.doi.org/10.15666/aeer/2402_24592501

ecological balances, contaminate drinking water supplies, hinder aquatic biodiversity, and even lead to the accumulation of toxins in the food chain (Thomas et al., 2014). Therefore, developing effective and sustainable dye removal technologies is crucial for mitigating the detrimental effects of dye pollution.

Nonetheless, industrial water pollution has been treated and removed using a variety of techniques, including conventional treatment methods like coagulation, flocculation, photocatalytic oxidation methods, membrane filtration, and chemical oxidation have been employed, these often face limitations, including high costs, generation of hazardous byproducts, and limited effectiveness against certain dye classes (Alprol, 2024). This has spurred researchers to explore alternative, environmentally friendly, and cost-effective approaches for dye removal. Adsorption, a widely recognized and versatile technique for contaminant removal, has emerged as a promising method for dye treatment (Abdallah and Alprol, 2024a). It involves the physical and chemical interactions between dye molecules and the surface of a solid adsorbent material. These interactions can include electrostatic attraction, hydrogen bonding, van der Waals forces, and π-π interactions, leading to the accumulation of dye molecules onto the adsorbent's surface (Al-Ajji and Al-Ghouti, 2021). In this study, the synthesis of activated carbon doped with zinc oxide and ammonia material (AC-ZnO-NH_3) composites have emerged as a novel and promising composite for dye removal from wastewater. Activated carbon, a highly porous and surface-area-rich material, has proven to be an effective adsorbent for removing various pollutants, including dyes, due to its exceptional ability to capture and retain contaminants (Usman et al., 2022). However, the adsorption capacity of activated carbon can be further enhanced by incorporating modifications and functionalization strategies. Doping with metal oxides, such as zinc oxide (ZnO), has shown significant promise in improving activated carbon's adsorption efficiency and expanding its applicability for dye removal (Zikalala et al., 2022).

In this study, Box-Behnken Design (BBD), one of the Response Surface Methodology (RSM) was applied for the optimization of process parameters in removal Acid red 1 dye from aquatic solution because it has a number of advantages such as: (i) estimation of the factors of the quadratic model (ii) detect lack of fit of the model (iii) avoids treatment combinations that are extreme (corner points or star points) i.e. BBD looks more desirable if the points are at the mid-point of edges of the process and at the center (Das and Mishra, 2017).

This study aims to investigate the potential of AC-ZnO-NH_3 nanocomposite for the removal of Acid Red 1 dye from aqueous solutions using a BBD approach. The influence of important factors, such as adsorbent dosage, contact time, dye concentration, and pH, on the effectiveness of dye removal will be methodically investigated. Additionally, FTIR, EDX, and SEM studies were used to assess the synthesis of AC-ZnO-NH_3 nanocomposite. To maximize dye removal with this new nanocomposite material, the ideal conditions must be ascertained by examining the interaction effects of various parameters. In addition to determine the efficacy and selectivity of the AC-ZnO-NH_3 composite against a broader range of waterborne pathogens to clarify the specific roles it in the antimicrobial activity (*Fig. A1*).

Materials and methods

Preparation of the activated carbon-zinc oxide-ammonia composite (AC-ZnO-NH_3)

The AC-ZnO-NH_3 composite was synthesized using a controlled impregnation and thermal activation method. Initially, 70 g of chemically activated carbon was mixed with

http://www.aloki.hu ● ISSN 1589 1623 (Print) ● ISSN 1785 0037 (Online)
DOI: http://dx.doi.org/10.15666/aeer/2402_24592501

15 g of ZnO nanoparticles in a glass beaker and stirred continuously for 30 min using a magnetic stirrer to ensure homogeneity. Subsequently, 50 mL of ammonia solution (10–20% v/v) was added dropwise to the mixture under continuous stirring. The resulting suspension was allowed to react at room temperature for 2 h, followed by thermal treatment at 80–100°C for 2 h to enhance nitrogen doping while preventing ammonia decomposition. After completion of the reaction, the mixture was vacuum-filtered and washed repeatedly with distilled water to remove unreacted species and residual ammonia.

The obtained solid was dried in an oven at 100°C for 12 h. Finally, the dried composite was thermally activated in a muffle furnace at 400°C for 1 h to improve surface area and porosity. The resulting material was stored in a desiccator prior to characterization and adsorption experiments.

Preparing the AR1 dye solution and chemicals

Accurate dissolution of AR1 dye in distilled water produced an initial dye concentration of 25–75 mg/L. By adding either 0.1% HCl or 0.1% NaOH, the pH was raised. Using a UV spectrophotometer (UV-1100 chrom Tech), the AR1 dye concentration was measured both before and after adsorption at wavelength λmax = 530 nm. The dye solution's concentration and absorbance were calibrated using a calibration curve. While the molecular formula ($C_{18}H_{13}N_3Na_2O_8S_2$) and the chemical structure of Acid Red 1 dye (*Fig. A2*).

Activated carbon with a purity of ≥ 99%. ZnO nanoparticles with a purity of ≥ 99.5% and ammonia solution with a purity of ≥ 28-30% (laboratory grade). HCl and NaOH with a purity of ≥ 99% (analytical grade). AR1 dye with a purity of ≥ 95% prevents interference with experimental results.

Adsorption study

In the batch adsorption studies, 50 mL of AR1 dye solution in range 10–50 mg/L containing varying amounts of (adsorbent composite) (0.01-0.03 g) was used, along with varying beginning dye concentrations. Using a shaker set to 200 rpm, the composite and AR1 dye solution was combined at 25°C at intervals of 30 to 90 min. After the adsorption period was completed, the dye solution was centrifuged at 3000 rpm for 10 min, and the remaining adsorbent was then filtered out using filter paper. *Equation 1* was used to get the AR1% and *Equation 2* was used to determine the quantity of dye adsorbed per gram of adsorbent at equilibrium time and at time t, respectively:

$$\text{AR1 Removal (\%)} = \frac{(Ci - Cf)}{Ci} \times 100 \quad \text{(Eq.1)}$$

$$q_e = \frac{(Ci - Cf) \times V}{W} \quad \text{(Eq.2)}$$

where: the concentration is represented by the symbols C_i and C_f are the liquid-phase concentrations of acid red 1 dye in mg/L at initial and equilibrium, respectively. In contrast, q_e is the maximum adsorption at monolayer (mg/g). The mass of the adsorbent is (W) with gram and the volume of the solution is V (L). The use of filter paper in the adsorption process plays a role in separating the remaining adsorbent material after the adsorption period. According to the study, after mixing the adsorbent composite and AR1

http://www.aloki.hu ● ISSN 1589 1623 (Print) ● ISSN 1785 0037 (Online)
DOI: http://dx.doi.org/10.15666/aeer/2402_24592501

dye solution, the mixture was centrifuged, and the remaining adsorbent was filtered out using filter paper. This filtration step ensures the removal of residual adsorbent particles from the solution, enabling accurate measurements of dye concentration before and after adsorption. It prevents interference from suspended particles during UV spectrophotometric analysis, providing precise data on adsorption efficiency.

Box-Behnken design (BBD)

The main purpose of the design of the experiment is to find out the common relationship between the multiple process variables in order to determine the optimum operating conditions for the system. It is also essential that the design methodology should be economical as well as it should also reduce experimental time to save both material and personnel cost (Vaez et al., 2012). The approach to process optimization is based on Response Surface Methodology (RSM), specifically using the Box-Behnken Design (BBD), which evaluates the interactions between process variables to identify optimal operating conditions efficiently (Wu et al., 2024).

Response surface methodology (RSM) is an efficient statistical method useful for modelling and analysis of the problem (Gottipati and Mishra, 2010). Box-Behnken design (BBD), a widely used form of RSM, was employed in the experimental procedure. The total number of experimental runs (N) was determined using Design- Expert Software, Version 7.0 (Stat-Ease, Minneapolis, USA). The equations generated by the Response Surface Methodology (RSM) using the Box-Behnken Design (BBD) (Gottipati and Mishra, 2010):

$$N = 2k\,(k - 1) + C_0 \qquad \text{(Eq.3)}$$

Where: k is the number of factors and C_0 is the number of central points. A second order polynomial regression model equation was used to express the predicted response (Y) as a function of independent variables which is expressed by *Equation 4*.

$$Y = \beta_{\mathcal{O}} + \sum_{i=\mathcal{I}}^{k} \beta_i x_i + \sum_{i=\mathcal{I}}^{k} \beta_{ii} x_i^2 + \sum_{i=\mathcal{I}}^{k-\mathcal{I}} \sum_{j=i+\mathcal{I}}^{k} \beta_{ij} x_i x_j \qquad \text{(Eq.4)}$$

where: $\beta_0, \beta_i, \beta_{ij}$ are the regression coefficients (β_0 is a constant term which corresponds to the response when the value of x_i is zero for each parameter, β_i is the linear effect term, $\beta_i$is the square effect term, β_{ij} is the interactive effect term and xi; xj are the variables that represent the important parameters affecting the characteristic of the process being carried out). ANOVA is used to estimate the statistical significance of the main effects and interactions, coefficients and residues that provides an overall summary for the full model (Vaez et al., 2012). In the present research work, a 4 factor of BBD was used for RSM to evaluate the effects and interactions of process parameters i.e. pH, AR1 dye Concentration, Adsorbent dosage and Contact time on the AR1 dye adsorption. The selected AR1 dye concentration range (25–75 mg/L) was chosen to simulate typical dye concentrations found in textile wastewater and to ensure adequate evaluation of adsorption performance under different loading conditions within the Box–Behnken experimental design. The ranges and levels of the independent variables are given in *Table 1*.

In this experimental design, input factors were set and these levels are called ‘high’ and ‘low’ and medium or ‘+1’ and ‘-1’ and ‘0’ respectively. The total number of experimental runs (N) was 29 runs and determined using Design- Expert Software,

http://www.aloki.hu ● ISSN 1589 1623 (Print) ● ISSN 1785 0037 (Online)
DOI: http://dx.doi.org/10.15666/aeer/2402_24592501

Version 7.0 (Stat-Ease, Minneapolis, USA) and the BOX matrix for method factors with tests for Acid Red 1 dye removal is shown in *Table 2*. After selecting four independent variables at three levels, the Box–Behnken Design matrix was automatically generated using Design-Expert software. The software-defined experimental design resulted in 29 experimental runs, including replicated center points, ensuring statistical efficiency and reliable estimation of linear, quadratic, and interaction effects while minimizing the total number of experiments. In accordance with Response Surface Methodology requirements, the mean values were used as the single response input for each experimental run in the Box–Behnken design.

Table 1. *Level of parameters in Box-Behnken experimental design*

Sample	Parameters	Unit	Minimum	Medium	Maximum
A	pH		3	5	8
B	AR1 Dye Conc.	mg/l	25	50	75
C	Adsorbent dosage	g	0.01	0.02	0.03
D	Contact time	min	30	60	90

Table 2. *Experimental design matrix and results*

Run	pH	Dye conc.	Adsorbent dosage	Contact time	Percentage removal %
1	-1	0	1	0	95.96
2	-1	0	0	1	99.75
3	-1	0	-1	0	79.19
4	-1	1	0	0	99.44
5	-1	0	0	-1	98.77
6	-1	-1	0	0	30
7	0	0	-1	1	44.39
8	0	-1	1	0	94.69
9	0	0	1	-1	40.73
10	0	1	1	0	99.40
11	0	1	0	1	48.46
12	0	0	0	0	30.10
13	0	0	0	0	37.98
14	0	-1	-1	0	64.37
15	0	-1	0	1	84.21
16	0	1	0	-1	36.52
17	0	0	0	0	49.54
18	0	0	1	1	84.32
19	0	0	-1	-1	41.64
20	0	1	-1	0	89.71
21	0	-1	0	-1	22.8
22	0	0	0	0	76.65
23	0	0	0	0	79.86
24	1	-1	0	0	40.08
25	1	1	0	0	31.67
26	1	0	-1	0	21.17
27	1	0	0	1	38.18
28	1	0	0	-1	76.66
29	1	0	1	0	40.26

http://www.aloki.hu ● ISSN 1589 1623 (Print) ● ISSN 1785 0037 (Online)
DOI: http://dx.doi.org/10.15666/aeer/2402_24592501

Desirability function

It is a popular approach for assessing the simultaneous optimization of the multiple responses having various input variables. It involves the conversion of each predicted response Yi, into an individual desirability function, di, on the basis of researcher's priorities and desires while building the optimization procedure (Varala et al., 2016). Which Xi, Ui and Zi be the lower, upper and target values that are designed for the response Yi with Xi < Yi < Ui. If the response is to be maximized, then the individual desirability(di) is defined as shown in *Equation 5* (Varala et al., 2016).

$$\text{di} = 0 \text{ if } \text{Yi} < \text{Xi } \text{di} = \left(\frac{Y_i}{z_i}\frac{-X_i}{-X_i}\right)^P \quad \text{(Eq.5)}$$

$$\text{If} = \text{Xi} < \text{Yi} < \text{Zi } \text{di} = 1 \text{ if } \text{Y1} > \text{Zi} \quad \text{(Eq.6)}$$

where: i and p are the weights. The desirability function varies over the range as shown in *Equation 5* with di = 0 indicating the undesirable value of Yi and di = 1, if the response achieves the target value (0 < di < 1). Thus, the individual desirability is then combined in order to maximize the overall desirability D, $D = (d1 \times d2 \times \ldots dm)^{1/m}$ with m denoting the no. of responses and d1; d2; dm are the desirability of the various responses. In this work, Box-Behnken design was applied with desirability approach in order to optimize the AR1 dye adsorption were desired to be at maximum levels. Once the maximum value of D is found, the optimal conditions are obtained.

Examination of isotherm and kinetic models

Equilibrium data should be carefully fitted into different isotherm models, and the equations plot of Freundlich, Langmuir, Tempkin and Harkins-Jura model isotherms were presented in *Table A1*. The adsorption kinetics of Acid Red 1 dye onto the composite material by applying five different kinetic models: Lagergren first-order, pseudo second-order, intraparticle diffusion, and Elovich models (the equation was shown in *Table A2*). In order to perform batch sorption tests at room temperature approximately 25–30°C, was mixed with 50 ml of AR1 and left at pH 3 a solution containing 10, 20, 30, and 40 mg/L for 3 h for measure isotherm and while for kinetic models the contact time was applied at 10, 20, 30, 60, 120 and 240 min at 40 mg/L. The reaction mixture was then analyzed to determine the amount of residual AR1content.

Characterization

Energy dispersive X-ray analysis (EDX) analysis (using the JEOL JSM-IT200 instrument) and a scanning electron microscope (SEM) were used to evaluate the morphology and elemental composition of the composite material composed. The particles of various sizes were calculated by JEOL JSM-IT200 instrument. The magnification of the image is ×40,000. This is indicated by the text "SED". Standard-PC 11.7 mm 30.0 High Vac; 20.0 kV WD. A Bruker IFS 66v/S spectrometer (Germany) and an IR Affinity -1S-SHIMADZU spectrometer (Kyoto, Japan) were used to get the powder sample's FTIR spectra. FTIR spectra were recorded using attenuated total reflection (ATR), with a resolution of 4 cm^{-1} and scans in the 4000-400 cm^{-1} spectral region. Zeta Potential Nanoparticle Analyzer (HORIBA Scientific SZ-100, UK) was used to measure the zeta potential. The thermogravimetric analysis (TGA) was performed to evaluate the

http://www.aloki.hu ● ISSN 1589 1623 (Print) ● ISSN 1785 0037 (Online)
DOI: http://dx.doi.org/10.15666/aeer/2402_24592501

thermal stability and decomposition profile of the AC-ZnO-NH_3 composite. The sample were analyzed using a TGA instrument (PerkinElmer Pyris 1 TGA) at 25°C to 800°C, at 10°C/min.

Antimicrobial activity assay

The antibacterial activity of the AC-ZnO-NH_3 composite was evaluated using the well diffusion method on Mueller–Hinton agar (MHA). The following bacterial strains were used as test organisms: *Staphylococcus aureus* (ATCC 25923). *Escherichia coli* (ATCC 8731), *Pseudomonas aeruginosa* (ATCC 9027), *Vibrio damsela*, *Klebsiella pneumoniae* (ATCC 13883), *Enterococcus faecalis* (ATCC 29212), *Vibrio fluvialis*, *Streptococcus agalactiae* and *Aeromonas hydrophila.* Bacterial suspensions were prepared from fresh overnight cultures and adjusted to a turbidity of 0.5 McFarland standard using a spectrophotometer at 600 nm. MHA plates were uniformly inoculated with each bacterial suspension using sterile cotton swabs. Wells with a diameter of 6 mm were punched into the agar, and 50 µL of the AC-ZnO-NH_3 composite suspension (prepared in distilled water at a concentration of X mg/mL) was added to each well. The plates were then incubated at 37°C for 24 h. After incubation, the diameters of the inhibition zones, including the well diameter, were measured in millimeters. All assays were performed in triplicate, and the mean values ± standard deviation were reported. Sterile distilled water and a known antibiotic (ampicillin) were used as negative and positive controls, respectively.

Statistical methods and software

All experimental data were statistically analyzed to ensure reliability and reproducibility. Response Surface Methodology (RSM) based on Box–Behnken Design (BBD) was applied to evaluate the individual and interactive effects of process variables, including pH, dye concentration, adsorbent dosage, and contact time, on Acid Red 1 dye removal efficiency. Analysis of variance (ANOVA) was employed to assess the statistical significance of the model terms and interactions at a confidence level of 95% ($p < 0.05$). Model adequacy was evaluated using regression coefficients (R^2, adjusted R^2, predicted R^2), F-values, p-values, adequate precision, lack-of-fit tests, and variance inflation factors (VIF). Kinetic and isotherm parameters were obtained using linear regression analysis. Thermodynamic parameters ($\Delta G°$, $\Delta H°$, and $\Delta S°$) were calculated using Van't Hoff equations based on adsorption data collected at different temperatures. All statistical modeling and optimization analyses were performed using Design-Expert software (Version 7.0, Stat-Ease Inc., Minneapolis, USA). Graphical data analysis and plotting were carried out using standard scientific data processing tools.

Cost estimation methodology

The cost estimation of the AC-ZnO-NH_3 composite was conducted based on a laboratory-scale production approach. The required quantities of activated carbon, ZnO nanoparticles, and ammonia solution were calculated according to the exact mass ratios and volumes employed during the synthesis procedure described in Section 2.1. Specifically, material consumption was derived from the preparation of a single batch using 70 g of activated carbon, 15 g of ZnO nanoparticles, and 50 mL of ammonia solution, and then normalized to cost per gram of the final composite. Market prices of the raw materials were obtained from certified chemical suppliers and standard laboratory

http://www.aloki.hu ● ISSN 1589 1623 (Print) ● ISSN 1785 0037 (Online)
DOI: http://dx.doi.org/10.15666/aeer/2402_24592501

reagent catalogs commonly used in academic research (e.g., Sigma-Aldrich, Merck, and local laboratory chemical distributors). Prices correspond to analytical- or laboratory-grade materials and reflect average market values at the time of the study. The cost estimation did not include labor, energy consumption, or equipment depreciation, as the analysis aims to provide a comparative material-level cost assessment rather than a full techno-economic evaluation. This methodology enables a realistic estimation of material cost and facilitates comparison with previously reported adsorbents synthesized under similar laboratory-scale conditions.

Results and discussion

Characterization of adsorbent material

SEM of AC-ZnO-NH₃ composite

SEM allows for direct visualization of the surface features, revealing the overall texture, particle size, and shape of the material. This information is essential for understanding the material 's properties and potential applications. The SEM image was acquired at a magnification of ×400 as presented in *Figure 1*.

The composite exhibits a porous structure, as evidenced by the presence of numerous interconnected pores and cavities. This porosity is likely attributed to the AC-ZnO-NH₃ component, which is known for its high surface area and porous nature (Joshi et al., 2021). The pores may contribute to the material's adsorption properties, potentially enhancing its effectiveness in capturing pollutants or other target molecules. The surface of the composite appears rough and uneven, indicating the presence of various features, including small particles and irregular shapes. This roughness may enhance the material's surface area, further contributing to its adsorption capabilities (Dubey et al., 2015). The particles in the composite exhibit a wide range of sizes, as indicated by the varying particle diameters marked in the image. The particles range in size from approximately 14 to 33 µm, suggesting that the synthesis process resulted in a non-uniform distribution of particle sizes. This heterogeneity may affect the overall performance of the composite, as smaller particles can potentially provide a larger surface area for interactions with target molecules.

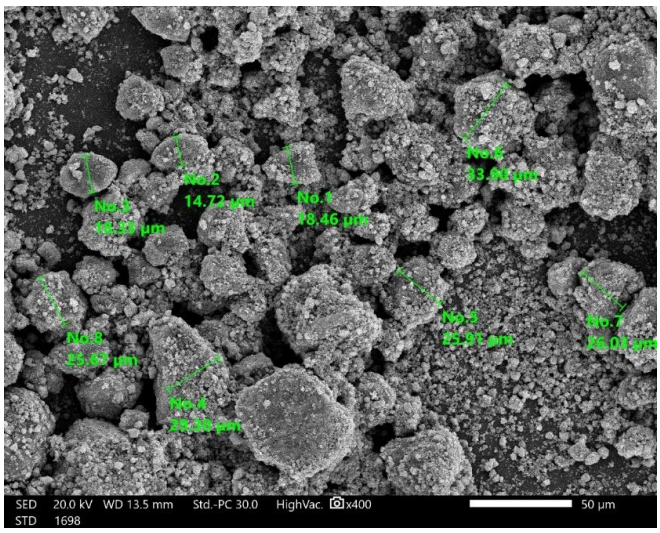

Figure 1. *SEM analysis of AC-ZnO-NH₃ composite*

http://www.aloki.hu ● ISSN 1589 1623 (Print) ● ISSN 1785 0037 (Online)
DOI: http://dx.doi.org/10.15666/aeer/2402_24592501

Elemental composition and EDX analysis

The EDX analysis reveals the elemental composition of the AC-ZnO-NH$_3$ composite, showing the following main elements and their respective mass and atomic percentages as presented in *Figure 2*. For example, carbon (C) has 26.84% by mass, 42.21% by atoms this indicates the presence of the activated carbon backbone, which provides the high surface area and porous structure essential for adsorption. Oxygen (O) has 39.35% by mass, 46.45% by atoms this high oxygen content suggests the presence of various oxygen-containing functional groups on the carbon surface, such as hydroxyl (-OH), carboxyl (-COOH), and carbonyl (C = O) groups. These groups play a crucial role in the adsorption process by providing binding sites for the dye molecules. Additionally, oxygen is present in the zinc oxide (ZnO) component. Also, iron (Fe) metal has 27.77% by mass, 9.39% by atoms this significant presence of iron suggests the potential presence of iron oxide (FeO) nanoparticles within the composite. Iron oxide can also contribute to adsorption, particularly by enhancing the composite's surface charge and acting as a catalytic agent for dye degradation. Correspondingly, zinc (Zn) metal with 4.45% by mass, 1.29% by atoms this confirms the presence of zinc oxide, a well-known semiconductor material with excellent adsorption properties. ZnO nanoparticles contribute to the composite's overall adsorption capacity by providing additional active sites for dye adsorption (Alprol et al., 2023). While, calcium (Ca) 1.09% by mass, 0.51% by atoms. The presence of calcium might indicate the inclusion of calcium-based materials or impurities in the synthesis process. While calcium might not be a major contributor to the adsorption, its presence should be considered when analyzing the overall properties of the composite. Besides, copper (Cu) has 0.50% by mass, 0.15% by atoms. The presence of copper could be due to impurities in the starting materials or the inclusion of copper-based materials during synthesis.

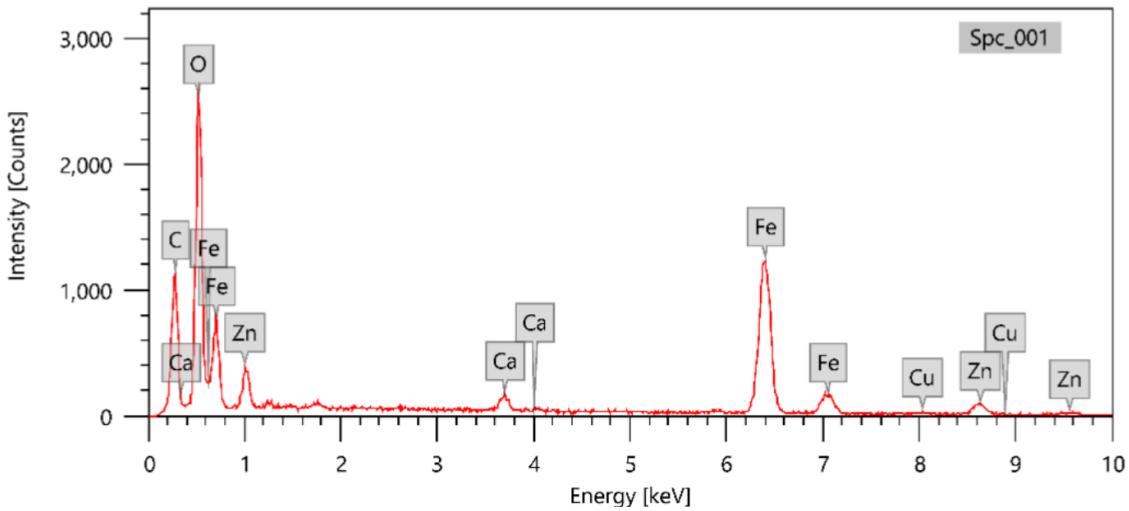

Figure 2. *EDX analysis of AC-ZnO-NH$_3$ composite*

Fourier transform infrared analysis

The FTIR data in *Figure 3a, b* for AC-ZnO-NH$_3$ nanocomposite indicates the presence of various functional groups, suggesting a complex chemical composition. For example, the peaks at 3856.086 and 3755.013 cm^{-1} are O-H stretch (surface hydroxyl groups)

http://www.aloki.hu ● ISSN 1589 1623 (Print) ● ISSN 1785 0037 (Online)
DOI: http://dx.doi.org/10.15666/aeer/2402_24592501

(Marchessault et al., 1960). Hydroxyl groups on the surface of the activated carbon can form hydrogen bonds with the dye molecules. This interaction is crucial for enhancing adsorption, especially for dyes with polar groups. While, the band at 3406.948 cm^{-1} show N-H stretch (amines). Amines are basic functional groups and can interact electrostatically with the negatively charged sulfonate groups present in Acid Red 1 dye. This electrostatic attraction promotes adsorption. C-H stretch (aromatic compounds) was found at 3135.737 cm^{-1}. Aromatic rings can interact with the aromatic rings present in Acid Red 1 dye through π-π stacking interactions. This interaction contributes to enhanced adsorption by increasing the contact area between the dye and the adsorbent. C-O stretching, one of the characteristic peaks of the carboxylic group, was correlated with the weak absorption bands observed at 2375.7 cm^{-1} (Anand and Suresh, 2015). Although, the C = C stretch (aromatic compounds) was confirmed at 1611.317 cm^{-1} which the aromatic structures on the activated carbon can interact with the dye through π-π stacking. Though, the band at 1399.661 cm^{-1} show C-N stretch (amines), this peak similar to the N-H stretch, C-N bonds in amines can also participate in electrostatic interactions with the dye. In addition, the peak at 889.036 cm^{-1} is C-H bending (aromatic compounds). This peak further supports the presence of aromatic structures, which play a crucial role in π-π stacking with the dye. The signal at 793.903 cm^{-1} for C-H bending (aliphatic compounds). While not as strong as hydrogen bonding or electrostatic interactions, van der Waals forces between the aliphatic carbon-hydrogen bonds on the activated carbon and the dye can contribute to adsorption. The peaks at 427.131 cm^{-1} display Zn-O stretching (ZnO). The presence of ZnO introduces a new dimension to the adsorption process. ZnO surfaces can interact with the dye through mechanisms like electrostatic interactions, hydrogen bonding, or even Lewis's acid-base interactions. ZnO's high surface area and potential catalytic properties can also contribute to adsorption efficiency. Additionally, ZnO typically exhibits a strong peak around 500 cm^{-1}, corresponding to the Zn-O stretching vibrations besides, the morphology of numerous peaks changes, especially at wavenumber ≈ 500 cm^{-1}, indicating the presence of (Zn–O) stretching of ZnO nanoparticles. Literature from the past has shown that low wavenumber (400–800 cm^{-1}) is where metal oxides stretching vibration bands are found (Jain et al., 2020). *Figure 3b* showed the adsorption of AR1 after treatment by AC-ZnO-NH_3, this figure indicate the significant decrease in absorption at 3853 cm^{-1} and 3743 cm^{-1}, indicating a reduction in -OH and -NH groups, highlighting their interaction with the compound during treatment. A major drop in absorption at 3395 cm^{-1}, showing consumption of amine groups or breakdown of associated structures. New peaks at 1579 cm^{-1}, 1499 cm^{-1}, and 1405 cm^{-1}, indicating the formation of new compounds or binding of absorbed material to the support (AC-ZnO-NH_3). Disappearance or reduction at 2375 cm^{-1}, suggesting the interactions with C = O groups. In the range of 2600-2550 showed the presence of S-H (thiol) stretching (Kadam et al., 2020). Correspondingly, stable peaks at 891 cm^{-1} and 589 cm^{-1}, indicating reduced aromatic effects while retaining some aromatic structures. Before treatment, peaks showed high intensities (up to 0.986), reflecting large quantities of dye. After treatment, intensities decreased in most peaks, indicating reduced dye concentration and pollutant absorption. After treatment, peaks became broader (e.g., 801.37 cm^{-1} compared to 625.484 cm^{-1}), reflecting chemical interactions between the absorbed material and the compound. Lower values in some locations indicate improved efficiency of the absorbent material in reducing high dye concentrations and transforming them into other compounds. Nonetheless, sulfur exists in sulfonate groups ($-SO_3^-$), which stabilize the dye structure and promote water

http://www.aloki.hu ● ISSN 1589 1623 (Print) ● ISSN 1785 0037 (Online)
DOI: http://dx.doi.org/10.15666/aeer/2402_24592501

solubility. After treatment, the range in 1415-1380 showed the originate of S = O stretching for sulfate or sulfonyl chloride. The decrease in absorption at 1399 cm^{-1} indicates breakdown or modification of sulfonate groups. Zinc oxide (ZnO) acts as a catalyst to oxidize sulfonate groups into sulfates (SO_4^{2-}) that dissolve or form insoluble residues on the composite material (Beig et al., 2023). Some sulfur may transform into gaseous products like SO_2 or H_2S under oxidative or thermal conditions (Awasthi et al., 2024).

Sodium ions balance the charge of sulfonate groups. After treatment sodium ions are likely released into the solution as Na^+ during the breakdown of sulfonate bonds. These ions remain in the solution or are removed through washing and filtration steps. After treatment the decrease in absorption at 1611 cm^{-1} and 1579 cm^{-1} suggests cleavage or oxidation of azo and amine groups. Nitrogen may convert into NO_3^- (nitrate) or NH_4^+ (ammonium) ions, or release volatile compounds like NH_3 (ammonia) (Das et al., 2009). Before treatment, oxygen (O) found in carboxyl (-COOH) and sulfonate (-SO_3H) groups, contributing to dye polarity (Fonseca et al., 2022). But, after treatment the changes in absorption at 3406 cm^{-1} and 3395 cm^{-1} indicate disruption of hydrogen bonding and removal of adsorbed water. Oxygen reacts with ZnO or radicals to form stable oxides or peroxides. ZnO generates reactive oxygen species (e.g., ˙OH) that attack organic bonds, breaking aromatic structures and azo bonds (-N = N-) (Bailon-Ruiz et al., 2023). ZnO generates •OH radicals that break bonds (C = C, -N = N-) and degrade the dye into simpler components (Ramaprabha and Kumar, 2025). In addition, ZnO oxidizes sulfur to sulfates and nitrogen to nitrates, stabilizing harmful groups as non-toxic forms (Ramaprabha and Kumar, 2025).

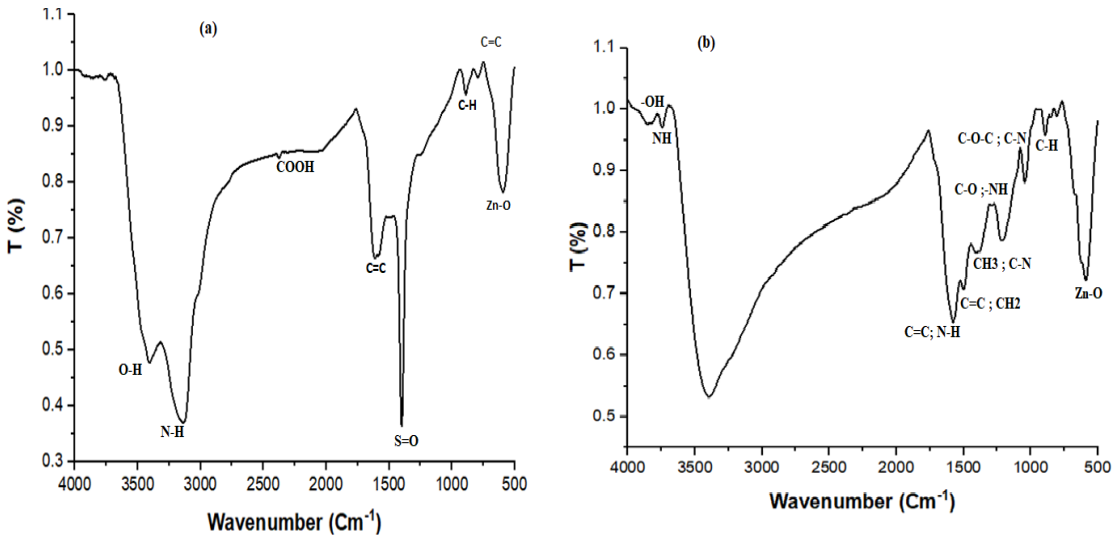

Figure 3. *Fourier transform infrared (FTIR) spectroscopy of adsorption of AR1 before (a) and after treatment (b) by AC-ZnO-NH₃*

Thermogravimetric analysis (TGA) of AC-ZnO-NH₃ composite

Thermogravimetric Analysis (TGA) was used to study the thermal stability and decomposition patterns of the AC-ZnO-NH_3 composite. Based on the material's composition, the results in *Figure 4* multiple stages of weight loss during the TGA analysis. Moisture loss below 150°C reflects the removal of physically adsorbed water

http://www.aloki.hu ● ISSN 1589 1623 (Print) ● ISSN 1785 0037 (Online)
DOI: http://dx.doi.org/10.15666/aeer/2402_24592501

and volatile organic compounds. This stage is typical for porous adsorbent materials like activated carbon and does not affect the structural integrity of the composite. The major weight loss between 150°C and 400°C can be attributed to the decomposition of organic compounds in the activated carbon structure. The ammonia doping introduces nitrogen-containing functional groups, such as amines (-NH_2), which decompose at relatively low temperatures, contributing to the observed weight loss. The functional groups identified in the FTIR analysis, including hydroxyl (-OH) and carboxyl (-COOH) groups, may also degrade during this phase. This region marks the thermal instability of the surface functional groups responsible for dye adsorption. At 400°C to 600°C, the remaining carbonaceous materials gradually decompose. ZnO nanoparticles, on the other hand, exhibit excellent thermal stability, which is reflected in the relatively minor weight loss in this temperature range. This result aligns with previous studies indicating that ZnO can withstand high temperatures without significant degradation. Residual weight (30%-35%) at temperatures above 600°C is primarily due to ZnO, which remains stable up to the maximum temperature studied (800°C). This residual mass confirms the presence of thermally stable metal oxides in the composite. ZnO nanoparticles, known for their high surface area and strong interaction with dye molecules, retain their structure at elevated temperatures, contributing to the composite's overall durability.

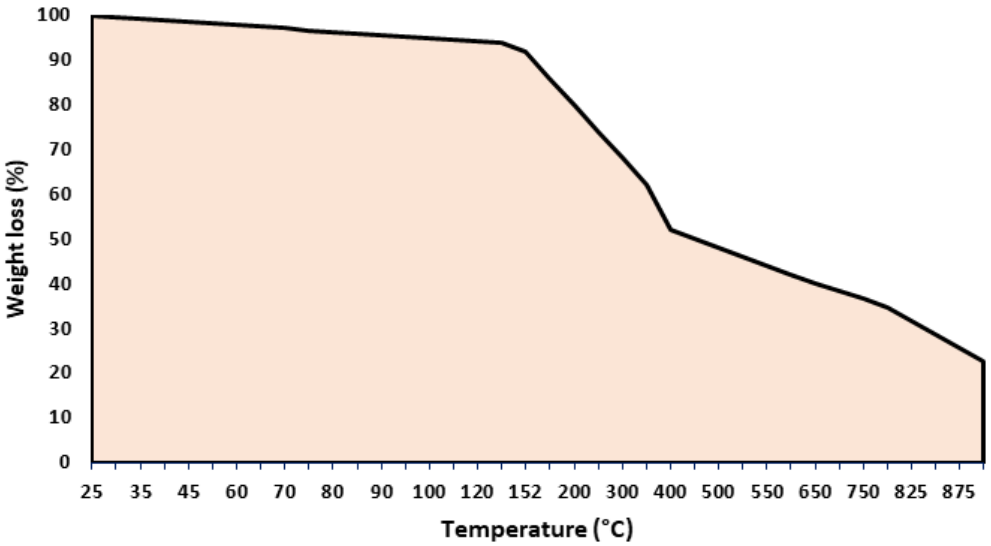

Figure 4. *Thermogravimetric analysis (TGA) of AC-ZnO-NH$_3$ composite*

Analysis of UV-Vis spectroscopy results for Acid Red 1 dye

UV-Vis spectroscopy graphs show the absorption spectra of Acid Red 1 dye before and after treatment using a Multifunctional Activated Carbon Doped with Zinc Oxide and Ammonia Composite. The spectra display absorbance (Abs) versus wavelength (nm). The results showed that before treatment with Acid Red 1 dye, two prominent peaks (signals) were observed at 300–350 nm which attributed to $\pi \rightarrow \pi^*$ transitions in aromatic rings and C = C or C = N bonds. While at range 500–550 nm is related to the azo (-N = N-) chromophore group responsible for the dye's red color. High absorbance in the visible region suggests a high concentration of intact dye molecules. The spectrum confirms the presence of the dye in its unaltered form, with no significant degradation or adsorption before treatment.

http://www.aloki.hu ● ISSN 1589 1623 (Print) ● ISSN 1785 0037 (Online)
DOI: http://dx.doi.org/10.15666/aeer/2402_24592501

While, after treatment of Acid Red 1 dye, significant reduction in absorbance across the entire wavelength range. The peak at 300–350 nm is diminished or partially disappeared, suggesting degradation or structural modification of aromatic rings. Also, the peak at 500–550 nm is dramatically reduced, indicating the breakdown of the azo chromophore group or dye removal through adsorption. The treated sample shows evidence of degradation or adsorption of the dye molecules, particularly targeting chromophoric and aromatic structures. The sharp decrease in peak intensity after treatment suggests effective degradation or adsorption of the dye molecules. Overall lower absorbance indicates a significant reduction in dye concentration, confirming successful removal. The azo group (500–550 nm) is either broken down chemically or adsorbed onto the composite material, reducing its optical signature.

Antimicrobial activity of AC-ZnO-NH₃ composites against waterborne pathogens

The presence of pathogens in water poses a significant public health risk, emphasizing the need for effective disinfection methods like the one explored in this study. The bacterial species included in this study are known to cause various waterborne illnesses in humans. For example: *Staphylococcus aureus c*auses skin infections, food poisoning, and serious infections like pneumonia. *Escherichia coli c*an lead to diarrhea, urinary tract infections, and other gastrointestinal illnesses. *Pseudomonas aeruginosa* is known for causing respiratory infections, wound infections, and sepsis. *Vibrio damsela c*an cause vibriosis, a potentially fatal seafood poisoning. *Klebsiella pneumoniae* is *a* common cause of pneumonia, urinary tract infections, and sepsis. *Enterococcus faecalis* is is frequently responsible for urinary tract infections and endocarditis. *Vibrio fluvialis a*ssociated with gastroenteritis and wound infections. *Streptococcus agalactiae c*auses neonatal infections, bacteremia, and meningitis. *Aeromonas hydrophila* **c**an cause gastroenteritis, wound infections, and septicemia.

Consequently, the data presented in *Table 3* reveals a differential antimicrobial effect of the AC-ZnO-NH_3 composites against a range of waterborne bacterial species. Notably, the composites demonstrated significant sensitivity towards *Staphylococcus aureus* and *Streptococcus agalactiae*, both gram-positive bacteria. Conversely, *Escherichia coli*, *Vibrio damsela*, *Klebsiella pneumoniae*, *Enterococcus faecalis*, and *Vibrio fluvialis* exhibited resistance, while *Pseudomonas aeruginosa* and *(Aeromonas hydrophila)* displayed intermediate sensitivity. These results suggest a potential for the AC-ZnO-NH_3 composite as a selective antimicrobial agent targeting certain bacterial species. The observed antimicrobial activity likely stems from a multi-pronged mechanism of action attributed to the composite's components: the porous structure of AC provides a large surface area for adsorption of bacterial cells. This physical entrapment can hinder bacterial growth and prevent their spread (Khamkeaw et al., 2020). ZnO exhibits potent antibacterial properties. It releases zinc ions (Zn^{2+}) that can disrupt bacterial cell membranes, leading to cell leakage and death. Furthermore, ZnO nanoparticles can generate reactive oxygen species (ROS) upon exposure to UV or visible light, causing oxidative stress and cell damage (Nath et al., 2023). Ammonia, a weak base, can raise the pH of the surrounding environment, potentially hindering the growth of some bacteria that thrive in acidic conditions. The differential sensitivity observed in this study may be linked to variations in cell wall composition, membrane permeability, and susceptibility to oxidative stress among the bacterial species (Lund et al., 2014). Gram-positive bacteria, with their thicker peptidoglycan layer, may be more susceptible to the disruption caused by ZnO and the adsorption properties of AC.

http://www.aloki.hu ● ISSN 1589 1623 (Print) ● ISSN 1785 0037 (Online)
DOI: http://dx.doi.org/10.15666/aeer/2402_24592501

Table 3. *Sensitivity of various bacterial species to AC-ZnO-NH₃ composites*

Bacterial species	Sensitivity	Gram staining	Inhibition zone diameter (mm)⁺
Staphylococcus aureus ATCC 25923	Sensitive	Gram-positive	14 ± 1.2
Escherichia coli ATCC 8731	Resistant	Gram-negative	6 ± 0.5
Pseudomonas aeruginosa ATCC 9027	Intermediate sensitivity	Gram-negative	9 ± 0.8
Vibrio damsela	Resistant	Gram-negative	5 ± 0.4
Klebsiella pneumoniae ATCC 13883	Resistant	Gram-negative	6 ± 0.6
Enterococcus faecalis ATCC 29212	Resistant	Gram-positive	5 ± 0.5
Vibrio fluvialis	Resistant	Gram-negative	5 ± 0.3
Streptococcus agalactiae	Highly sensitive	Gram-positive	18 ± 1.5
Aeromonas hydrophila	Intermediate sensitivity	Gram-negative	10 ± 1.0

Sensitive: Inhibition zone diameter ≥ 12 mm; Intermediate: Inhibition zone diameter 9–11 mm; Resistant: Inhibition zone diameter ≤ 8 mm

Surface response of AR1 dye adsorption

Design Expert software was utilized in this study to statistically analyze all results. *Table 2* displays the findings of the experimental design for the removal %, encompassing 29 runs. *Table 2* illustrates that the actual percentage of dye removal was acquired from studies that are roughly in line with the developed model's expected values. The results and determine optimal conditions for maximizing the removal of Acid Red 1 dye showed that run 2 (99.75%) achieved the highest removal percentage. The run was conducted at pH 3 (low), Dye Concentration 50 mg/L (medium), Adsorbent dosage 0.01 g (low), and Contact Time 90 min (high). Meanwhile, the run 21 (22.8%) achieved the lowest removal percentage. This run was conducted at pH 5 (medium), dye concentration 25 mg/l (low), Adsorbent dosage 0.02 g (medium), and contact time 30 min (low). It was evident that the highest removal percentage had the longest contact time (90 min). The suggests that longer contact times allow more dye molecules to interact with the adsorbent, leading to higher removal. The lowest removal percentage had a neutral pH (5). A pH of 3 might be more conducive to adsorption. Acidic conditions often favor the removal of anionic dyes like Acid Red 1.

In this work, Box-Behnken Design (BBD), a form of RSM, was employed to optimize the removal of Acid Red 1 dye. BBD facilitated systematic evaluation of interactions between these variables and identified conditions (e.g., pH 5, 0.03 g adsorbent dosage, 90 min) that maximized dye removal efficiency. The results showed high correlation coefficients, validating the applicability of RSM for modeling and predicting adsorption performance. Another study RSM was employed to optimize the adsorption conditions for Cu^{2+} removal using pottery sludge (Uddin et al., 2018). Box-Behnken Design (BBD) efficiently identified optimal operating conditions, saving experimental resources (Beg and Akhter, 2021). RSM successfully modeled the adsorption process with a high correlation coefficient between predicted and experimental results.

Interaction effects of process variables on responses

Figures 5–9 show the interaction of different parameters on the removal of Acid Red 1 dye using AC-ZnO-NH_3 composite from aqueous solutions. These figures were generated using a Box-Behnken design (BBD) model, a statistical technique used to

http://www.aloki.hu ● ISSN 1589 1623 (Print) ● ISSN 1785 0037 (Online)
DOI: http://dx.doi.org/10.15666/aeer/2402_24592501

optimize complex processes. Each figure represents a 3D response surface plot, showing the interaction of two parameters while keeping the other two constant. *Figure 5a* shows the interaction of pH and Acid Red 1 dye concentration on the dye removal efficiency. This figure indicates that the dye removal efficiency increases with increasing pH, while the effect of dye concentration is more complex. At low pH levels, the dye removal efficiency is relatively low, but it increases significantly with increasing pH. However, at higher dye concentrations, the dye removal efficiency starts to decrease again. As documented in the literature, this effect is more typical for cationic and anionic dyes (Deniz and Saygideger, 2011). *Figure 5b* shows the interaction of pH and adsorbent dosage on the dye removal efficiency. This indicates that the dye removal efficiency increases with increasing adsorbent dosage and pH. The increasing adsorbent dosage means a higher number of active sites to adsorb the Acid Red 1 dye from the solution. This is an expected result, as the increase in adsorbent dosage provides more surface area for adsorption, leading to higher dye removal efficiency (Abdallah and Alprol, 2024b). *Figure 6* demonstrates the interaction of contact time and pH on the dye removal efficiency. The figure indicates that the dye removal efficiency increases with increasing contact time and pH. The longer contact time allows the adsorbent to adsorb the Acid Red 1 dye more efficiently. The increasing pH also contributes to the higher dye removal efficiency.

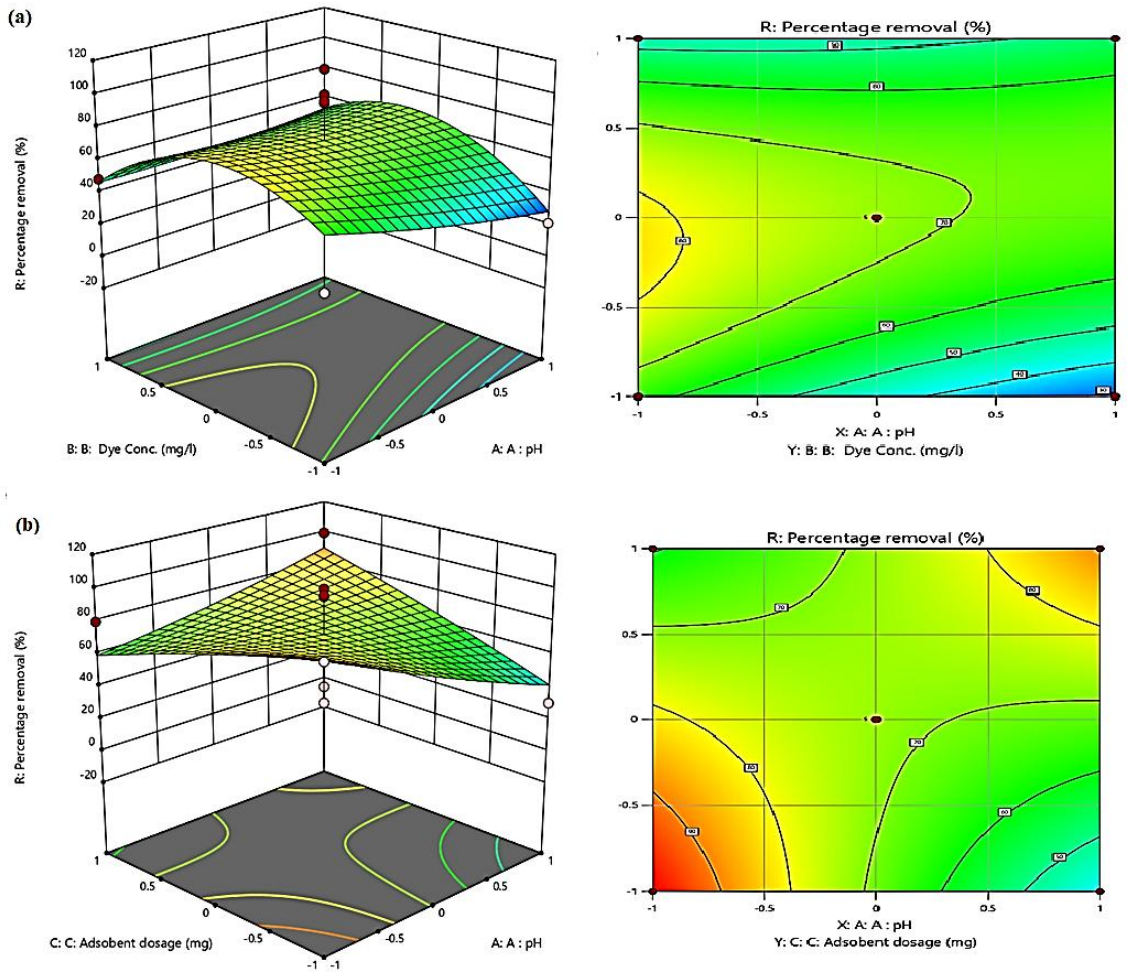

Figure 5. *Interaction of pH and Acid Red 1 dye concentration (a) and interaction of pH and adsorbent dosage (b)*

http://www.aloki.hu ● ISSN 1589 1623 (Print) ● ISSN 1785 0037 (Online)
DOI: http://dx.doi.org/10.15666/aeer/2402_24592501

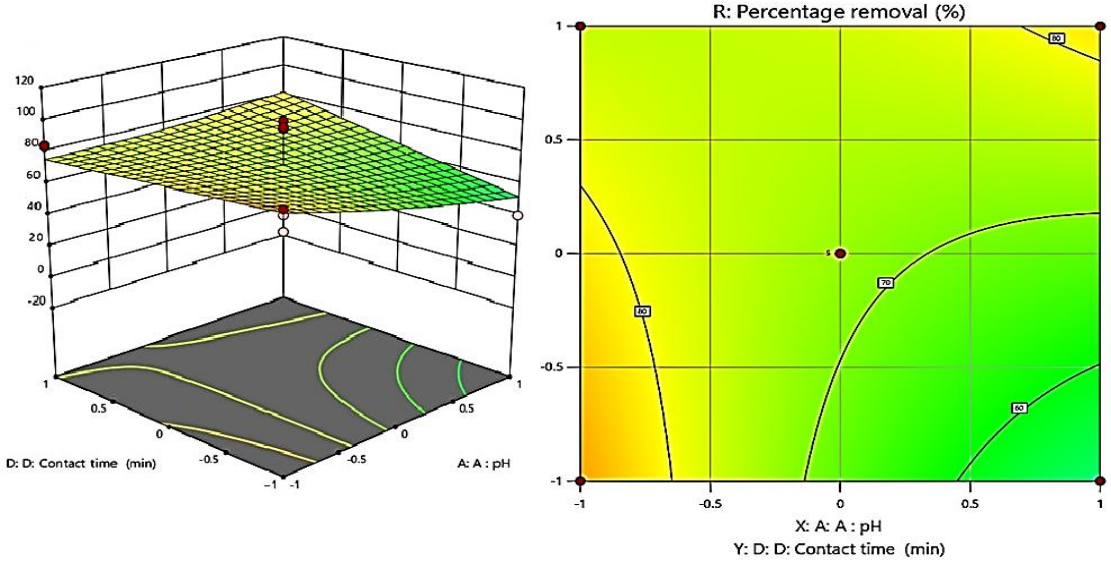

Figure 6. *Interaction of contact time (min) and pH*

Nevertheless, *Figure 7* shows the interaction of initial Acid Red 1 dye concentration and adsorbent dosage on the dye removal efficiency. The figure indicates that the dye removal efficiency decreases with increasing initial dye concentration but increases with increasing adsorbent dosage. The higher initial dye concentration means a higher competition for the adsorption sites on the AC-ZnO-NH_3, leading to a lower dye removal efficiency. On the other hand, increasing adsorbent dosage leads to a higher number of adsorption sites, resulting in a higher dye removal efficiency (Elzahar and Bassyouni, 2023).

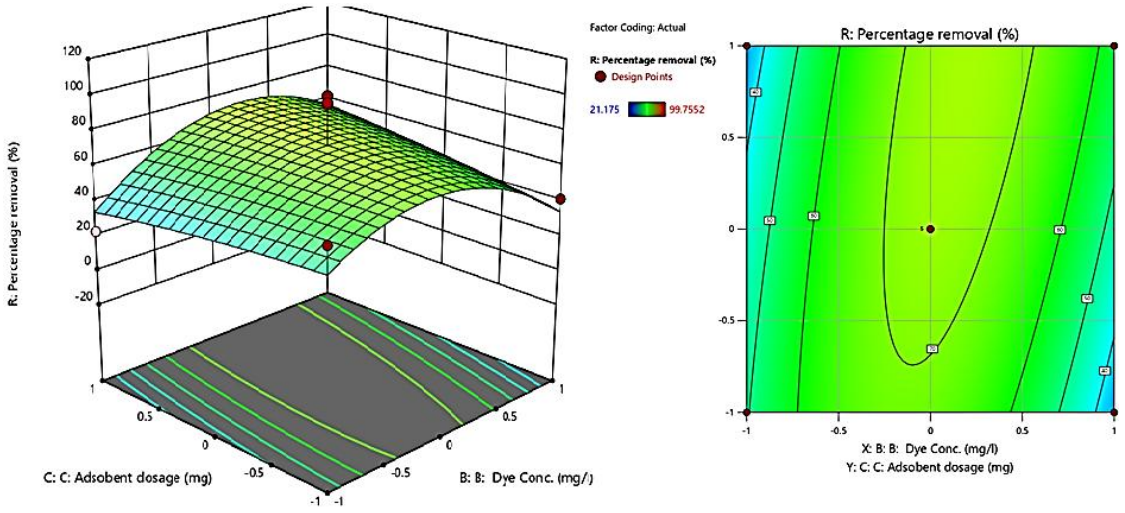

Figure 7. *Interaction of initial Acid Red 1 dye concentration and adsorbent dosage*

Figure 8 shows the interaction of contact time and Acid Red 1 dye concentration on the dye removal efficiency. The figure indicates that the dye removal efficiency increases with increasing contact time and decreases with increasing Acid Red 1 dye concentration. The longer contact time allows more dye to be adsorbed onto the surface of the AC-ZnO-NH_3, increasing the removal efficiency. However, as the dye concentration increases, the

http://www.aloki.hu ● ISSN 1589 1623 (Print) ● ISSN 1785 0037 (Online)
DOI: http://dx.doi.org/10.15666/aeer/2402_24592501

number of dye molecules competing for adsorption sites also increases, leading to decreased removal efficiency (Pelekani and Snoeyink, 2001).

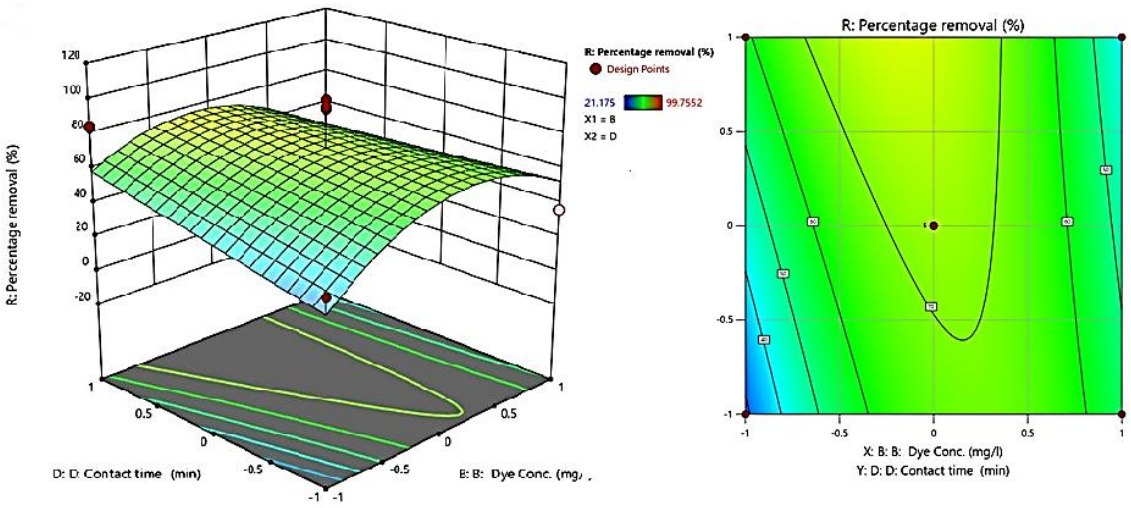

Figure 8. *Interaction of contact time and Acid Red 1 dye concentration*

Also, *Figure 9* shows the interaction of contact time and adsorbent dosage on the dye removal efficiency. The figure indicates that the dye removal efficiency increases with increasing contact time and adsorbent dosage. This is because the longer contact time allows more dye to be adsorbed onto the surface of the AC-ZnO-NH_3. The higher adsorbent dosage provides more active sites for adsorption, leading to a higher dye removal efficiency (Abualnaja et al., 2021a).

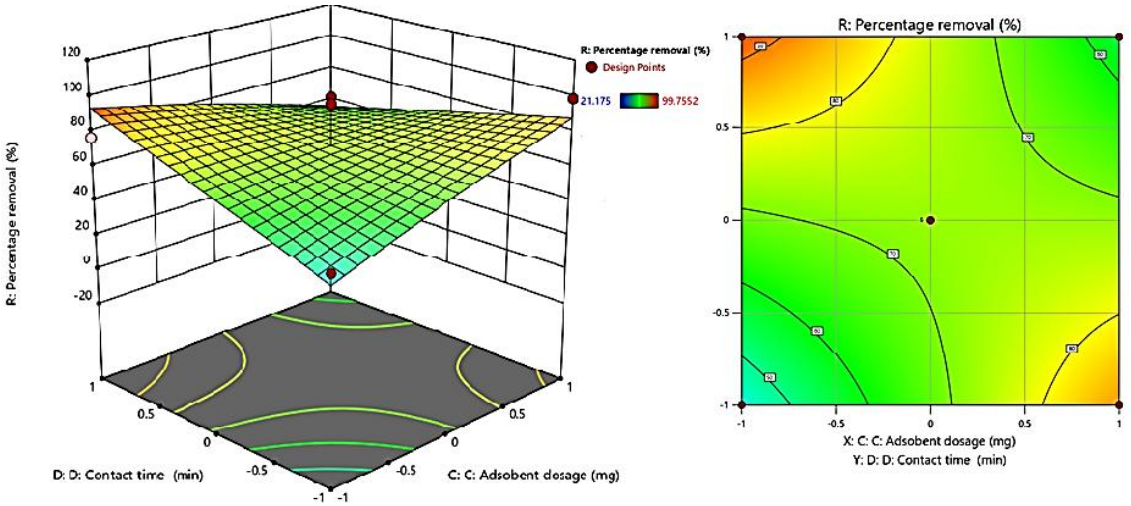

Figure 9. *Interaction of contact time and adsorbent dosage*

Analyzing the normal plot of residuals for Acid Red 1 adsorption

A normal distribution of residuals indicates that the model used to predict the adsorption values is appropriate. This is essential because a valid model allows for

http://www.aloki.hu ● ISSN 1589 1623 (Print) ● ISSN 1785 0037 (Online)
DOI: http://dx.doi.org/10.15666/aeer/2402_24592501

accurate predictions and reliable optimization of the adsorption process (Jayan et al., 2021). *Figure 10* is a normal plot of residuals; this type of plot is used to assess the normality of the residuals from a regression model. The red line represents a perfect normal distribution. Each point on the plot represents a residual (the difference between the actual value and the predicted value) from one of the 29 experimental runs. The plot shows that the majority of the points fall close to the diagonal line. This suggests that the residuals are approximately normally distributed. There is one point that deviates significantly from the line, indicating a potential outlier. The outlier suggests a potential problem with one of the experimental runs. Investigating this outlier could lead to improvements in the model or identifying errors in the experimental procedure.

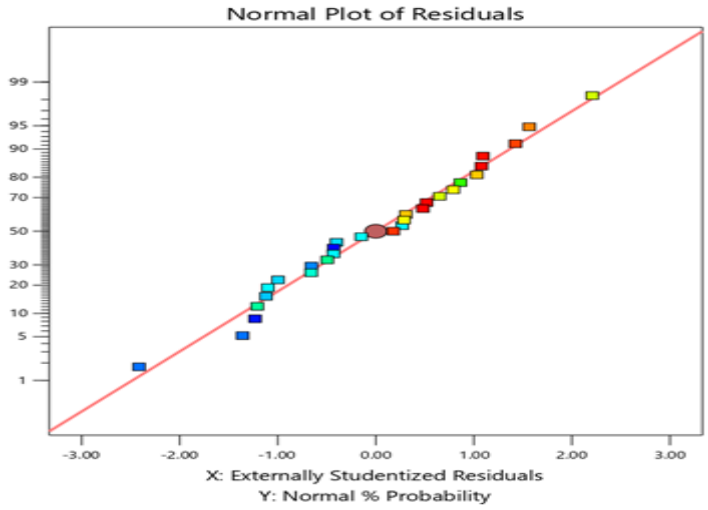

Figure 10. *Analyzing the normal plot of residuals for Acid Red 1 adsorption*

Process optimization

Figure 11 presents the results of a numerical optimization analysis performed using a Box-Behnken design (BBD) model. The analysis aimed to determine the optimal conditions for the adsorption of Acid Red 1 dye using AC-ZnO-NH_3 doped with zinc oxide and ammonia. The ramps in this figure ramps are graphical representations of the optimal solution for each of the four factors involved in the adsorption process: The ramp shows that the optimal pH is at the center point (0), meaning a neutral pH 5 is best for maximizing the dye removal efficiency. The optimal dye concentration was at the high end (1), indicating that a higher concentration of Acid Red 1 dye at 75 mg/L, leads to a better adsorption performance. The ramp shows the optimal adsorbent dosage is at that the highest at 0.03 g, that implying that a higher dosage of AC-ZnO-NH_3 material improves the dye removal efficiency. Meanwhile, the ramp shows the optimal contact time is also at that the high end (1), indicating that a longer contact time between the dye solution and the adsorbent is beneficial for efficient dye removal.

The numerical optimization ramps provide a numerical representation of the optimized process conditions. The values of 0.999 for Acid Red 1 dye concentration (BB), adsorbent dosage (CC), and contact time (DD) indicate that these factors are at their maximum possible levels for optimal performance. The value of -3.5783E-07 for pH (AA) suggests that a neutral pH is the most desirable for the adsorption process. Also, this figure shows

http://www.aloki.hu ● ISSN 1589 1623 (Print) ● ISSN 1785 0037 (Online)
DOI: http://dx.doi.org/10.15666/aeer/2402_24592501

the predicted response (R1) at the optimal conditions. The value of R1 = 83.4437 indicates a predicted dye removal efficiency of 83.4437%. This analysis suggests that a higher initial dye concentration, a higher dosage of the AC-ZnO-NH$_3$ material, and a longer contact time contribute to the efficient removal of Acid Red 1 dye. The pH of 5 is the most favorable for the adsorption process, likely because it minimizes any potential interference from the acidic or basic conditions that can affect the adsorption process.

The desirability value of 1.000 indicates that the optimal solution is highly desirable, as it maximizes the predicted dye removal efficiency (Das and Mishra, 2017). This value suggests that the optimized conditions effectively balance the different factors and provide the best possible result for the adsorption process.

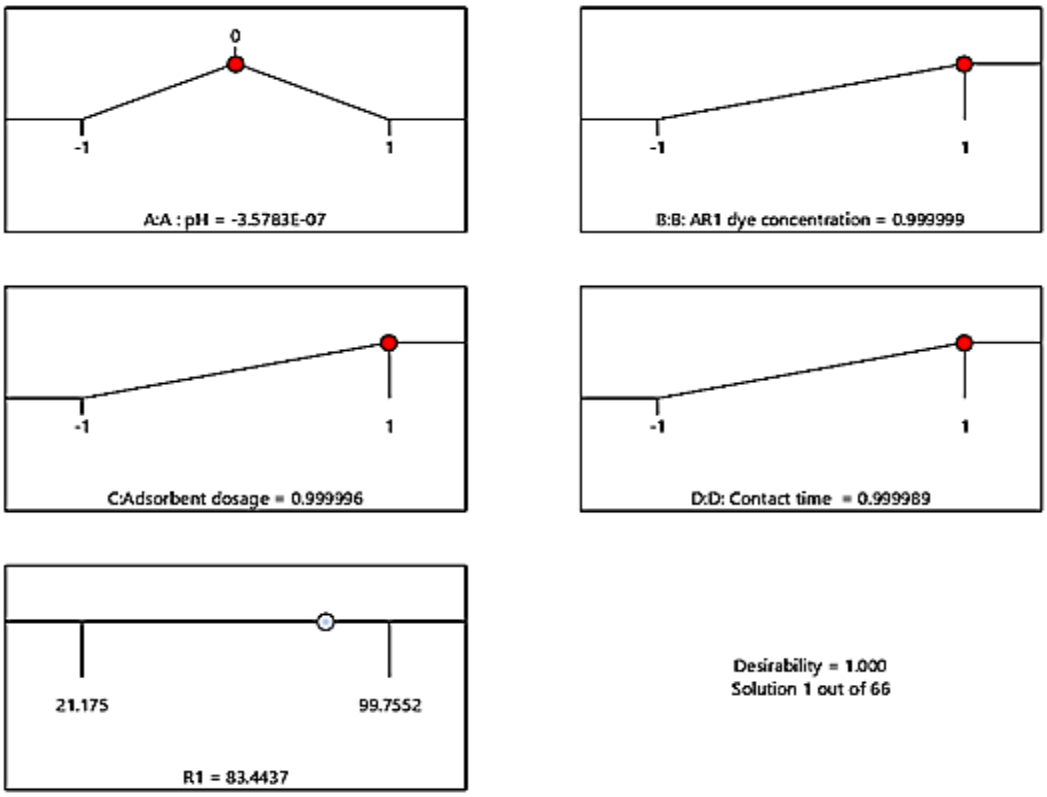

Figure 11. *Optimized process conditions*

Impact of each process variable perturbation on the dye removal efficiency

Figure 12 shows the desirability for (pH) parameter that moving away from the reference point in either direction (lower pH or higher pH) results in a decrease in desirability (likely meaning lower removal efficiency). The curve is steeper for lower pH, suggesting a more significant drop in efficiency as pH decreases. The curve flattens out for higher pH, indicating a less dramatic change in efficiency. As the dye concentration increases (moving to the right), the desirability decreases. This indicates that higher initial dye concentrations lead to lower removal efficiency. Meanwhile, as the adsorbent dosage increases (moving to the right), the desirability increases. This indicates that a higher dosage of adsorbent leads to higher removal efficiency. As the contact time increases (moving to the right), the desirability increases, suggesting that longer contact times result in better removal efficiency.

http://www.aloki.hu ● ISSN 1589 1623 (Print) ● ISSN 1785 0037 (Online)
DOI: http://dx.doi.org/10.15666/aeer/2402_24592501

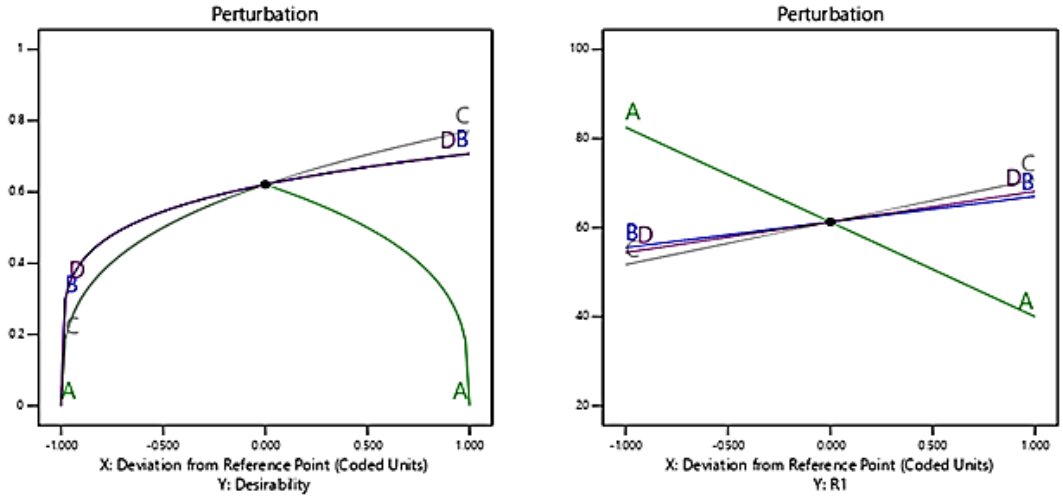

Figure 12. *Impact of each process variable perturbation on the dye removal efficiency*

Also, *Figure 12* shows a linear decrease in response variable (R1) likely removal efficiency as pH increases (moving to the right). This suggests that increasing pH negatively impacts the removal efficiency of the dye. It is showing a slight linear increase in R1 (removal efficiency) as dye concentration increases (moving to the right). However, the change is very small, indicating a minimal impact of dye concentration on removal efficiency. Because, the adsorbent dosage increases (moving to the right), R1 (removal efficiency) slightly increases. This suggests that a higher dosage of adsorbent leads to a slightly higher removal efficiency. As contact time increases (moving to the right), R1 (removal efficiency) increases. This suggests that longer contact times lead to better removal efficiency.

Spatial distribution of Acid Red 1 dye removal: insights from a Box-Behnken design and cube plots

Knowing the interplay between process variables is crucial for optimizing the removal of Acid Red 1 dye. This analysis, utilizing a Box-Behnken design, sheds light on the spatial variation of removal efficiency with respect to pH, dye concentration, and adsorbent dosage, revealing potential areas for process improvement (*Fig. 13*).

While, the actual Factor (D) for contact time parameter = -0.993 suggests a high level of agreement between the predicted and experimental values, indicating a good model fit. The cube desirability plot 2 visually shows the predicted desirability values (likely representing the overall process optimization) across different combinations of the process variables: pH, dye concentration, and adsorbent dosage. The desirability values are plotted on the cube's vertices, ranging from 0 to 0.000, indicating that the model predicts minimal desirability (likely indicating less-than-ideal removal efficiency) for all combinations of the process variables considered. This suggests that the current model might not be ideal for optimizing the process (Fernandes et al., 2020).

The cube R1 plot shows the predicted response variable (R1, as Acid Red 1 dye removal efficiency) across different combinations of pH, dye concentration, and adsorbent dosage. The removal efficiency varies significantly across different combinations of variables. For example, the highest removal efficiency is predicted at A + 1, B + 1, and C + 1, indicating a high removal efficiency when operating at higher

http://www.aloki.hu ● ISSN 1589 1623 (Print) ● ISSN 1785 0037 (Online)
DOI: http://dx.doi.org/10.15666/aeer/2402_24592501

pH, higher dye concentration, and higher adsorbent dosage. This is counterintuitive, as it typically expects higher dye concentration to negatively impact removal efficiency.

The cube standard error of R1 plot shows the standard error of the prediction for R1. It indicates the uncertainty associated with the predicted values. The standard error is relatively uniform across the cube, suggesting that the model's prediction uncertainty is consistent across the various process variable combinations (DeChant and Moradkhani, 2014). The cubical plots demonstrate that Acid Red 1 dye removal efficiency varies significantly across different combinations of pH, dye concentration, and adsorbent dosage. Increasing adsorbent dosage (C + 1) generally leads to higher removal efficiency, as expected.

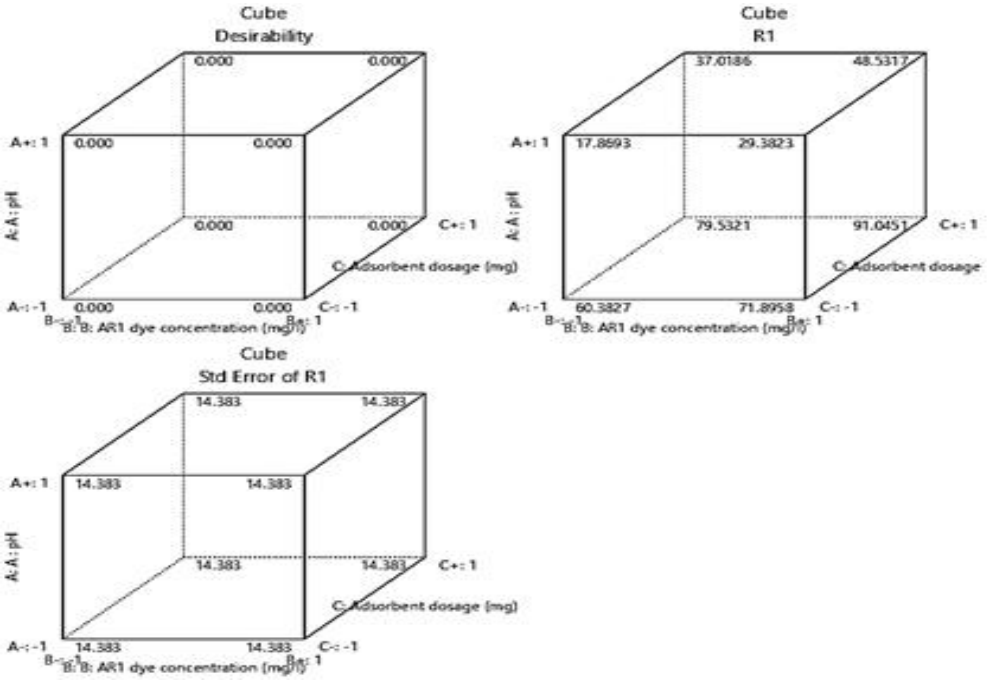

Figure 13. *Spatial distribution of Acid Red 1 dye removal by AC-ZnO-NH₃ composite*

Analysis of ANOVA

The ANOVA in *Table 4* shows that the linear model is statistically significant (F-value = 3.32, p-value = 0.0268), indicating a relationship between the independent variables (pH, dye concentration, adsorbent dosage, and contact time) and the response variable (percentage dye removal). The low p-value suggests a 2.68% chance of observing such a large F-value by random chance. However, only the pH variable (A) is significant with a p-value of 0.0049. While, the lack of fit F-value is 1.14 with a p-value of 0.5066, suggesting that the lack of fit is not significant. This indicates that the model fits the data well and there is no evidence of systematic error. The R-squared value of 35.6% suggests that the model explains a moderate amount of variability in the response. However, it is relatively low, indicating that there may be other factors influencing dye removal that are not accounted for in the model. The adjusted R-squared value of 0.2486 takes into consideration the number of terms in the model and provides a better measure of the model's predictive power. The predicted R-squared value of 0.0433 is significantly lower than the adjusted R-squared value, indicating potential issues with the model. This discrepancy could be due to a large

http://www.aloki.hu ● ISSN 1589 1623 (Print) ● ISSN 1785 0037 (Online)
DOI: http://dx.doi.org/10.15666/aeer/2402_24592501

block effect or problems with the data or model (Zhu et al., 2014). Further investigation is necessary to address this difference. The Adequate Precision value of 6.2527 is greater than 4, indicating an adequate signal-to-noise ratio. This suggests that the signal is strong enough to effectively use the model to navigate the design space. To further quantify the influence of each factor, partial eta-squared (η^2) was calculated as a measure of effect size. The results (*Table 4*) reveal that pH (Factor A) exhibits the largest effect size ($\eta^2 = 0.286$), which is classified as a large effect according to Cohen's guidelines. In contrast, dye concentration ($\eta^2 = 0.029$), adsorbent dosage ($\eta^2 = 0.075$), and contact time ($\eta^2 = 0.040$) showed small to medium effects. This confirms that pH is the most dominant factor in the adsorption process, consistent with its significant p-value ($p = 0.0049$) and substantial contribution to the total variance in dye removal efficiency.

Table 4. *Combined ANOVA summary for the linear model for Acid Red 1 dye removal, including effect size (partial η^2)*

Factor	Sum of squares	df	Mean square	F-value	p-Value	Partial η^2	Effect size interpretation
Model	7482.94	4	1870.73	3.32	0.026*	–	–
A (pH)	5422.18	1	5422.18	9.61	0.0049*	0.286	Large effect
B (Dye Conc.)	397.65	1	397.65	0.704	0.409	0.029	Small effect
C (Adsorbent Dosage)	1100.09	1	1100.09	1.95	0.175	0.075	Medium effect
D (Contact Time)	563.01	1	563.01	0.998	0.327	0.040	Small effect
Residual	13538.02	24	564.08	–	–	–	–
Lack of Fit	11511.67	20	575.58	1.14	0.5066	–	–
Pure Error	2026.35	4	506.59	–	–	–	–
Total	21020.96	28	–	–	–	–	–

Partial η^2 interpretation guidelines (Goulet-Pelletier and Cousineau, 2018): Small effect: $\eta^2 \approx 0.01$, Medium effect: $\eta^2 \approx 0.06$ and Large effect: $\eta^2 \geq 0.14$

The coefficient estimate for the significant factor pH (A) is -21.26, indicating a negative linear correlation with the response variable. This suggests that as pH increases, the percentage of dye removal decreases. The ANOVA analysis highlights pH as the most influential factor affecting dye removal in this system, likely due to its impact on the surface charge of the adsorbent material and the ionization state of the dye molecules. However, the low R^2 and discrepancies between the adjusted and predicted R^2 raise concerns about the overall fit of the model. The BBD design can capture quadratic effects, so including quadratic terms for all factors in the model may enhance the fit. Transforming the response variable could also improve the model's linearity and alignment with the data. Examining residuals for outliers can help identify and address any unusual data points that may be influencing the model. While the BBD provided valuable insights into the main effect of pH on dye removal, further refinement of the model is necessary to consider potential interactions, higher-order terms, and address issues with the model fit. *Table 4* show the model F-value of 3.32 implies the model is significant. There is only a 2.68% chance that an F-value this large could occur due to noise. P-values less than 0.0500 indicate model terms are significant. In this case A is a significant model term. Values greater than 0.1000 indicate the model terms are not significant. If there are many insignificant model terms (not counting those required to support hierarchy), model reduction may improve this model.

http://www.aloki.hu ● ISSN 1589 1623 (Print) ● ISSN 1785 0037 (Online)
DOI: http://dx.doi.org/10.15666/aeer/2402_24592501

The lack-of-fit test was employed to evaluate the adequacy of the developed quadratic model. The lack of Fit F-value of 1.14 implies the lack of fit is not significant relative to the pure error (*Table 4*). There is a 50.66% chance that a lack of fit F-value this large could occur due to noise. The obtained lack-of-fit was statistically non-significant ($p > 0.05$), indicating that the proposed model sufficiently represents the experimental data and that the residual error is primarily due to random experimental variations rather than model inadequacy. This confirms the reliability of the model for predicting Acid Red 1 dye removal under the investigated operating conditions. The predicted R^2 of 0.0433 is not as close to the adjusted R^2 of 0.2486 as one might normally expect; i.e. the difference is more than 0.2. This may indicate a large block effect or a possible problem with this model and/or data. Things to consider are model reduction, response transformation, outliers, etc. All empirical models should be tested by doing confirmation runs. Adeq-precision measures the signal to noise ratio. A ratio greater than 4 is desirable. The ratio of 6.253 indicates an adequate signal. This model can be used to navigate the design space. The coefficient estimate represents the expected change in response per unit change in factor value when all remaining factors are held constant. The intercept in an orthogonal design is the overall average response of all the runs. The coefficients are adjustments around that average based on the factor settings. When the factors are orthogonal the VIFs are 1; VIFs greater than 1 indicate multi-colinearity, the higher the VIF the more severe the correlation of factors. As a rough rule, VIFs less than 10 are tolerable as presented in *Table 4*.

Temperature effect and thermodynamic analysis

Temperature is critical in determining the feasibility and nature of adsorption processes. Lower temperatures favor adsorption by providing stability to physical forces, whereas higher temperatures may enhance mobility and desorption tendencies, making adsorption less effective (Sulaiman et al., 2021). The adsorption efficiency and adsorption capacity (Q_e) of Acid Red 1 dye decrease significantly as the temperature increases as showed in *Figure 14*. At 30°C, the adsorption process achieves the highest removal efficiency (94.697%) and adsorption capacity (125 mg/g). However, as the temperature increases to 40°C, 50°C, and 60°C, there is a sharp decline in both metrics. At 60°C, the removal efficiency drops drastically to 7.302% with a Q_e value of 11.50 mg/g. The process is more favorable at lower temperatures, suggesting that adsorption may be predominantly physical adsorption characterized by van der Waals forces or hydrogen bonding. Lower temperatures reduce the kinetic energy of dye molecules, allowing better interaction with the adsorbent surface (Shaheen and Hanif, 2024). Structural changes in the composite material or decreased affinity between the dye molecules and the adsorbent surface might occur at higher temperatures (Nannu Shankar et al., 2023). Also, the adsorption mechanism involves, electrostatic interaction, functional groups and pore filling. The porous structure of activated carbon provides high surface area and facilitates diffusion and entrapment of dye molecules.

Thermodynamic parameters provide insights into the nature, spontaneity, and feasibility of the adsorption process. The results in *Table 5* showed a positive value of enthalpy change ($\Delta H° = 138$ kJ/mol) indicates the process is endothermic, requiring energy input to sustain adsorption. Such a high $\Delta H°$ suggests strong interactions consistent with chemical adsorption rather than purely physical adsorption. The negative value of entropy change ($\Delta S° = -0.383$ J/mol/K) implies a decrease in randomness at the solid-liquid interface during adsorption, indicating organized dye

http://www.aloki.hu ● ISSN 1589 1623 (Print) ● ISSN 1785 0037 (Online)
DOI: http://dx.doi.org/10.15666/aeer/2402_24592501

molecule arrangement onto the adsorbent surface (Mustapha et al., 2019). Also, a positive ΔG° value of gibbs free energy change (ΔG° = 15.01 kJ/mol) suggests that the adsorption process is non-spontaneous under the studied conditions and requires external energy input to drive the process (Imla Syafiqah and Yussof, 2018). Besides, the large ΔH° value implies chemical adsorption involving stronger covalent or ionic bonding mechanisms, as opposed to physical adsorption based on weak van der Waals forces. The process is endothermic, as indicated by the positive ΔH°, meaning it favors lower temperatures for equilibrium.

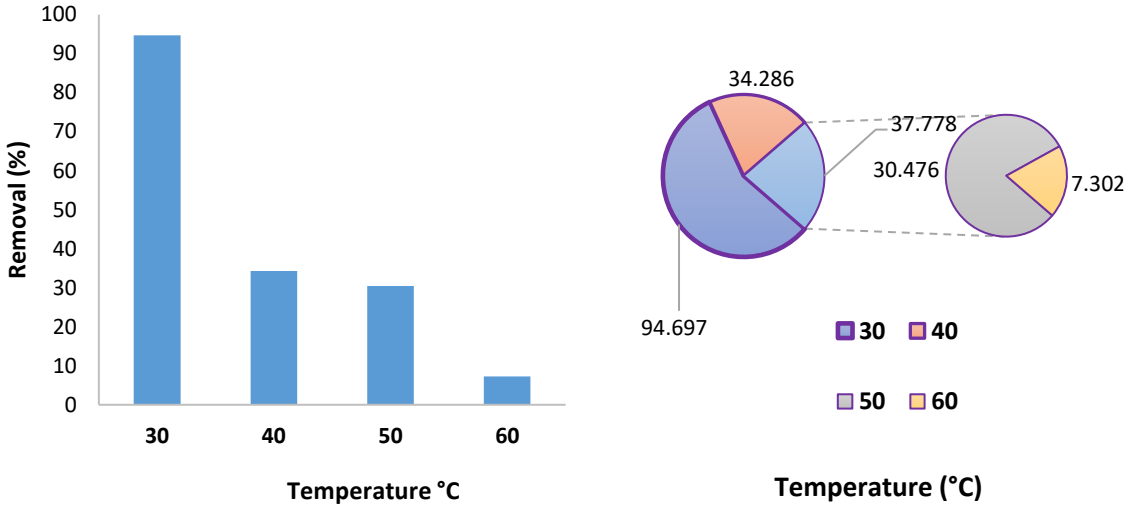

Figure 14. *Temperature effect of Acid Red 1 dye by onto AC-ZnO-NH₃ composites*

Table 5. *Thermodynamic analysis of Acid Red 1 dye by onto AC-ZnO-NH₃ composites*

Thermodynamic parameters	Value
ΔH° (kJ/mol)	138
ΔS° (J/mol/K)	-0.383
ΔG° (kJ/mol)	15.01

Mechanism of Acid Red 1 dye adsorption onto AC-ZnO-NH₃ composites

Chemical reactions and adsorption mechanisms

(a) Electrostatic interaction

In aqueous solutions, AR1 dye exists as a dianionic species (AR1) due to the deprotonation of its two sulfonate groups (-SO_3H) (Vázquez-Vélez et al., 2021). The AC-ZnO-NH_3 composite material possesses a net positive charge, largely attributed to the presence of ammonia (NH_3) which acts as a weak base, readily accepting protons (H^+) from water molecules, forming ammonium ions (NH_4^+). This creates a positively charged surface on the composite material. So, the electrostatic attraction between the negatively charged AR1 and the positively charged AC-ZnO-NH_3 composite drives the initial adsorption process as presented in the following equation.

$$C_{18}H_{13}N_3Na_2O_8S_2^{(-2)} + [\text{AC-ZnO-NH3}]^{(+n)} \rightarrow [C_{18}H_{13}N_3Na_2O_8S_2\text{-AC-ZnO-NH}_3]^{(+n-2)} \quad \text{(Eq.7)}$$

http://www.aloki.hu ● ISSN 1589 1623 (Print) ● ISSN 1785 0037 (Online)
DOI: http://dx.doi.org/10.15666/aeer/2402_24592501

where: $[AC\text{-}ZnO\text{-}NH_3]^{(+n)}$ represents the positively charged composite with a charge of ^{+}n, and $[AR1\text{-}AC\text{-}ZnO\text{-}NH_3]^{(+n-2)}$ is the adsorbed complex with a charge of ^{+}n-2.

(b) Hydrogen bonding

The sulfonate groups ($-SO_3^-$) and the azo groups (-N = N-) in AR1 dye contain oxygen atoms with lone pairs of electrons. The ammonia molecules (NH_3) attached to the composite have a lone pair of electrons on the nitrogen atom, capable of forming hydrogen bonds with the oxygen atoms of AR1. This hydrogen bonding contributes to the stability of the AR1-composite complex, enhancing its adsorption as presented in the following equation:

$$AR1\text{-}SO_3^- + NH_3 \leftrightarrow AR1\text{-}SO_3^- \ldots H\text{-}NH_2 \quad \text{(Eq.8)}$$

where: $AR1\text{-}SO_3^-$ represents the sulfonate group of the dye, NH_3 represents ammonia in the composite, and $AR1\text{-}SO_3(-) \ldots H\text{-}NH_2$ represents the hydrogen bond formed.

(c) π-π Interaction

The aromatic rings in AR1, particularly those containing the azo group (-N = N-), possess a significant electron density due to the delocalization of electrons within the π system. Activated carbon also exhibits a π-electron cloud structure (Sharma et al., 2022). This interaction between the π-electron clouds of the AR1 dye and the activated carbon surface enhances the adsorption process as presented in the following equation:

$$AR1 \text{ (aromatic ring)} + AC \text{ (aromatic ring)} \rightarrow AR1 \ldots AC \quad \text{(Eq.9)}$$

where: AR1 (aromatic ring) represents the aromatic ring of the dye, AC (aromatic ring) represents the aromatic structure of activated carbon, and AR1. Activated Carbon represents the π-π stacking interaction.

(d) Surface complexion

The sulfonate groups ($-SO_3^-$) in AR1 can undergo deprotonation at higher pH values, forming anionic species. Zinc oxide nanoparticles in the composite possess Lewis acidic sites on their surface. The anionic AR1 dye species can form surface complexes with the Lewis acidic sites on ZnO, leading to a more stable adsorption as presented in the following equation:

$$AR1^{(-2)} + ZnO \leftrightarrow [AR1\text{-}ZnO]^{(+n-2)} \quad \text{(Eq.10)}$$

where: $AR1^{(-2)}$ represents the dye anion, and $[AR1\text{-}ZnO]^{(+n-2)}$ represents the surface complex formed.

Isotherm model analysis

This study investigates the removal of Acid Red 1 dye from aqueous solution using $AC\text{-}ZnO\text{-}NH_3$ composites. The effectiveness of the composite material as an adsorbent is evaluated through sorption isotherm models, aiming to understand the mechanism and capacity of dye removal at different initial concentrations.

http://www.aloki.hu ● ISSN 1589 1623 (Print) ● ISSN 1785 0037 (Online)
DOI: http://dx.doi.org/10.15666/aeer/2402_24592501

Freundlich isotherm

This model assumes a heterogeneous surface with multiple adsorption sites having different binding energies (Freundlich, 1906). It describes multilayer adsorption, where the adsorption capacity increases with increasing concentration. A graph of log q_e vs. log C_e is plotted and the value of 1/n and K_f are calculated. The nature and intensity of the adsorption process, as well as the distribution of active sites, can be assessed through the slopes of the 1/n values. If $1/n = 1$, the partitioning between the two phases remains constant regardless of concentration. Adsorption is considered normal and follows the L-type Langmuir isotherm when $1/n < 1$, while cooperative adsorption, which indicates strong interactions between the adsorbate molecules, is observed when $1/n > 1$. In this study, 1/n values less than 1, suggesting that the adsorption of AR1 onto adsorbent follows a normal pattern, consistent with the typical L-type Langmuir isotherm (Sulaiman et al., 2021). *Table 6* presented the value of 1/n (0.397) indicates the intensity of adsorption, ranging from 0 to 1 suggests a favorable adsorption process. A value closer to 0 represents a more favorable adsorption. The parameter of Freundlich constant (k_f) indicates a relatively high adsorption capacity (de Franco et al., 2018). The low R^2 value (0.557) indicates a poor fit of the Freundlich model to the experimental data, suggesting that the model may not be the most suitable to describe the adsorption mechanism. This could be due to the presence of multiple adsorption mechanisms or the limitations of the model in representing complex adsorption processes.

Langmuir isotherm

Langmuir model assumes a homogeneous surface with a limited number of identical adsorption sites (Langmuir, 1917). It describes monolayer adsorption, where each site can bind only one adsorbate molecule. The slope and intercept of a plot of C_e/q_e vs. C_e are applied to define the values of q_m and b. *Table 6* presented the maximum adsorption capacity Q_m value of 312.5 mg/g indicates a high adsorption capacity of the AC-ZnO-NH_3 composite for Acid Red 1 dye. This supports the formation of a complete monolayer on the adsorbent surface, influenced by the varying functional groups on the adsorbent, which leads to maximum uptake capacities (Al Prol, 2019). Further analysis of the Langmuir isotherm can be conducted using the dimensionless separation factor (R_L). This factor is a key characteristic of the Langmuir model that describes the nature of the adsorption process. It is calculated using the following equation:

$$R_L = \frac{1}{1 + K_L C_0} \quad \text{(Eq.11)}$$

where: C_0 represents the initial concentration of the adsorbate in solution (mg/L), and K_L is the Langmuir constant. The interpretation of R_L values is as follows; the adsorption process is unfavorable if $R_L > 1$. It is favorable if $0 < R_L < 1$, the adsorption is linear if $R_L = 1$ and it is irreversible if $R_L = 0$. In this study (Amrutha et al., 2023), the separation factor (R_L) was found to be 0.175, indicating that the adsorption process was favorable and demonstrates the effectiveness of the adsorbent in removing the contaminant. Ka is Langmuir constant related to the energy of adsorption was initiate to be 28.419. The R^2 value of 0.966 suggests a good fit of the Langmuir model to the experimental data, indicating a possible monolayer adsorption mechanism. This suggests that the Langmuir model is a better representation of the adsorption process compared to the Freundlich

http://www.aloki.hu ● ISSN 1589 1623 (Print) ● ISSN 1785 0037 (Online)
DOI: http://dx.doi.org/10.15666/aeer/2402_24592501

model. This may indicate a significant role of monolayer adsorption on the surface of the composite material. This supports the formation of a complete monolayer on the adsorbent surface, influenced by the varying functional groups on the adsorbent, which leads to differences in maximum uptake capacities (Sahu et al., 2022).

Tempkin isotherm

Tempkin model considers the effect of heat of adsorption and assumes a linear decrease in the heat of adsorption with increasing surface coverage (Tempkin and Pyzhev, 1940). *Table 6* presents the value of A (2.71) is related to Tempkin constant related to the heat of adsorption. Higher values indicate stronger interactions between the adsorbate and the adsorbent surface. The value of B (32) reflects the desorption constant, which provides insights into the energy required for desorption to occur. Higher values of B may imply lower tendencies for desorption, thus favoring adsorption (Sulaiman et al., 2021). However, the low R^2 value of 0.567 suggests a poor fit of the Tempkin model to the experimental data, indicating that the model may not be suitable for describing the adsorption mechanism in this system. The Tempkin model assumes a linear decrease in the heat of adsorption, which might not be accurate for complex systems like the AC-ZnO-NH_3 composite. The moderate values of constants (A and B) imply the presence of interactions between adsorbate and adsorbent; however, the complexity of the surface chemistry and heterogeneity might require alternative models for better fitting.

Table 6. *Isotherm model analysis for removal of Acid Red 1 dye from aqueous solution using AC-ZnO-NH_3 composites*

Isotherm model	Parameter	Value
Freundlich	1/n	0.397
	k_f	49.773
	R^2	0.557
Langmuir	Qm	312.5
	R^2	0.966
	Ka*1000	28.419
	R_L	0.175
Tempkin	A	2.71
	B	32
	R^2	0.567
Harkins-Jura	AHJ	9.395
	BHJ	11.13
	R^2	0.533

Harkins-Jura isotherm

Harkins-Jura model is based on the assumption of multilayer adsorption on a solid surface with a non-uniform distribution of adsorption sites (Harkins and Jura, 1944). AHJ (9.395) represents the constant related to the surface area of the adsorbent, providing insights into the available adsorption sites. BHJ (11.13) describes the energy of adsorption, which determines how strongly the adsorbate molecules bind to the adsorbent (Abualnaja et al., 2021b) (*Table 6*). The low R^2 value of 0.533 suggests a poor fit of the

http://www.aloki.hu ● ISSN 1589 1623 (Print) ● ISSN 1785 0037 (Online)
DOI: http://dx.doi.org/10.15666/aeer/2402_24592501

Harkins-Jura model to the experimental data, indicating that the model may not be the most suitable to describe the adsorption mechanism. Besides, the low R^2 value suggests that the Harkins-Jura model may not be able to accurately capture the complex adsorption behavior of Acid Red 1 dye on the AC-ZnO-NH_3 composite. The constants (AHJ and BHJ) suggest some degree of multilayer adsorption, but the poor model fit highlights the limitations of applying Harkins-Jura for this composite material.

Figure 15 displays the linear equilibrium isotherms for the adsorption of Acid Red 1 onto the AC-ZnO-NH_3 composite. It shows the relationship between the equilibrium concentration of the dye in the solution (C_e) and the amount of dye adsorbed per unit mass of adsorbent (q_e). The figure compares the experimental data (q_e exp.) with the predictions of four different isotherm models: Freundlich, Langmuir, Tempkin, and Harkins-Jura.

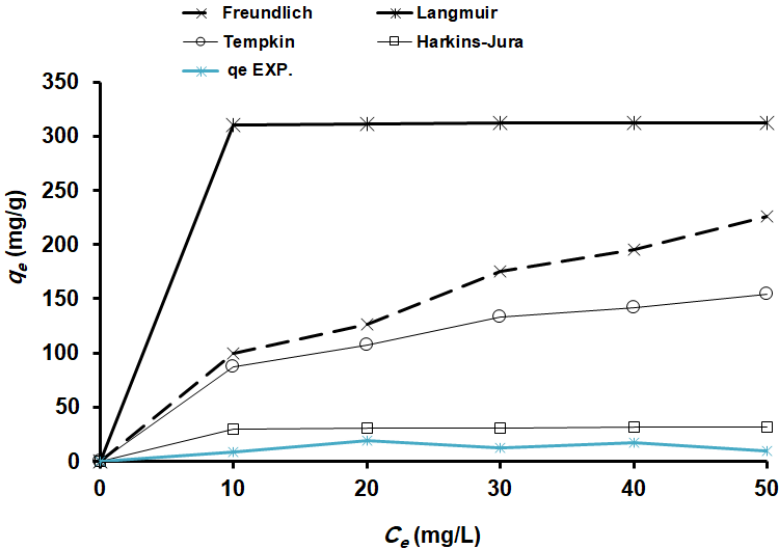

Figure 15. *The experimental of adsorption capacity and predicated adsorption capacity (q_e) for Freundlich, Langmuir, Tempkin and Harkins-Jura model isotherm*

The experimental data shows a gradual increase in the amount of dye adsorbed (q_e) with increasing initial dye concentration (C_e). However, the adsorption capacity seems to plateau around 30 mg/L, indicating that the AC-ZnO-NH_3 composite reaches its saturation point at higher concentrations. The Freundlich model predicts a continuous increase in adsorption with increasing concentration, fitting the experimental data well at lower concentrations. However, it overestimates the adsorption at higher concentrations, highlighting its limitations in capturing the saturation behavior observed in the experiment. The Langmuir model provides a good fit to the experimental data across the entire range of concentrations. The model predicts a plateau in adsorption at higher concentrations, aligning well with the experimental observation of a saturation point.

Adsorption kinetics of Acid Red 1 dye onto AC-ZnO-NH_3 composites

Understanding the rate and mechanism of dye removal using AC-ZnO-NH_3 composites is crucial for optimizing the adsorption process. This study investigates the adsorption kinetics of Acid Red 1 dye onto the composite material by applying five different kinetic models: Lagergren first-order, pseudo second-order, intraparticle diffusion, and Elovich models (*Table 7*).

http://www.aloki.hu ● ISSN 1589 1623 (Print) ● ISSN 1785 0037 (Online)
DOI: http://dx.doi.org/10.15666/aeer/2402_24592501

Table 7. *Adsorption kinetics parameters of Acid Red 1 dye onto AC-ZnO-NH₃ composites*

Model	Parameters	Results value
First-order kinetic model	Q_e (calc.)	1.59
	K1 × 10^3	5.75
	R^2	0.026
Second-order kinetic model	q_e (calculation)	38.910
	K_2 × 10^3	6.572
	R^2	0.994
	q_e (exp.)	41.400
Elovich isotherm model	β	1.594
	Intercept	38.99
	Ln (αβ)	62.185
	αβ	1.01533E + 27
	α	6.3661E + 26
	R^2	0.072
Intraparticle diffusion	K_{dif}	0.044
	C	41.051
	R^2	0.0056

Lagergren first-order kinetic model

Lagergren First-Order Kinetic model describes a first-order rate of adsorption based on the assumption that the adsorption rate is proportional to the number of vacant sites on the adsorbent (Samimi and Shahriari-Moghadam, 2023). A straight line is obtained by plotting log (q_e-q_t) versus t with a negative slope equal to K_1/2.303 and intercept equal to log q_e. The slope and intercept yield the values of k1 and q_e, respectively as presented in *Figure A3*. *Table 7* display the rate constant (k_1) value was 5.7 with higher values of k_1 indicate a faster adsorption rate, suggesting a strong affinity between the dye and the adsorbent (Al-Saeedi et al., 2023). In addition, the low R^2 value (0.0269) suggests a poor fit of the model to the experimental data, indicating that the first-order adsorption mechanism may not be dominant in this system. While, the calculated equilibrium adsorption capacity Q_e (1.59 mg/g) significantly deviates from the experimental value (41.4 mg/g). The poor fit suggests that the adsorption process is not solely controlled by the number of vacant sites on the adsorbent, implying the involvement of other factors such as diffusion or surface interaction.

Pseudo second-order kinetic model

Pseudo second-order (PSO) kinetic model proposes a second-order rate of adsorption based on the assumption that the adsorption rate is proportional to the square of the number of vacant sites (Bullen et al., 2021). A straight line can be obtained by plotting t/q_t versus t. The value of k_2 and q_e can be evaluated from the slope and intercept respectively (*Fig. 16*). It should be obvious that only when the adsorbate concentration fluctuates considerably can the PSO equation be used. The adsorption is seen to be a chemical process in this paradigm, and it happens when the adsorbent and the adsorbate share or exchange electrons. The rate constant K_2 was 6.572 g/mg/min, besides the high R^2 value (0.994) suggests a good fit of the model to the experimental data, indicating that

http://www.aloki.hu ● ISSN 1589 1623 (Print) ● ISSN 1785 0037 (Online)
DOI: http://dx.doi.org/10.15666/aeer/2402_24592501

the pseudo second-order mechanism may be significant in the adsorption process. Also, the higher values of k_2 signify a stronger interaction between the dye molecules and the adsorbent. Besides the calculated Q_e (38.91 mg/g) is close to the experimental value (41.4 mg/g), further supporting the model's applicability. The good fit suggests that the adsorption process might be dominated by the interaction between the dye molecules and the active sites on the composite material, with a strong dependence on the availability of vacant sites (Rezazadeh et al., 2020).

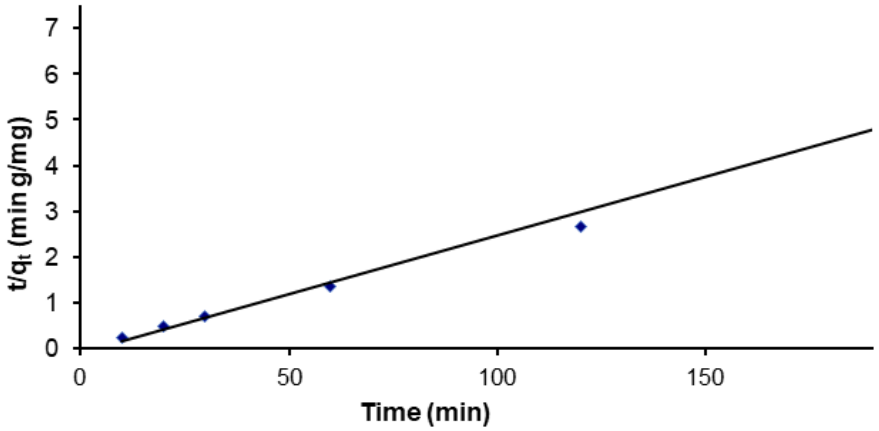

Figure 16. *Pseudo second-order kinetic model for AR1 adsorption on to AC-ZnO-NH₃ composites*

Intraparticle diffusion model

Intraparticle diffusion model assumes that the diffusion of the dye into the pores of the adsorbent is the rate-limiting step (Abd El-Hamid et al., 2022). It proposes a linear relationship between the adsorbed amount (q_t) and the square root of time ($t^{1/2}$). Intraparticle diffusion rate constant K_{dif} (mg/g/min$^{1/2}$) was presented in *Table 8* and *Figure A4*. The results showed a higher value of K_{dif} indicates faster diffusion of the dye into the adsorbent pores. K_{dif} = (0.044 mg/g/min$^{1/2}$) has low diffusion rate constant indicates slow penetration of the dye into the pores. While, the intercept value (C) can provide insights into the initial adsorption rate and the contribution of boundary layer diffusion. (41.051 mg/g) the intercept suggests a significant boundary-layer effect, implying external diffusion may influence adsorption.

The low R^2 value (0.0056) suggests a poor fit of the model to the experimental data, indicating that intraparticle diffusion may not be the sole rate-limiting step. The low R^2 value suggests that other factors, such as film diffusion or surface interaction, might also play a role in controlling the overall adsorption rate. Plots that were obtained did not go through the origin. This demonstrated that there were additional kinetic parameters influencing and contributing to the pace and mechanism of AR1 dye adsorption onto adsorbent, confirming that the intraparticle diffusion model was not the sole step that limited the rate (Lin et al., 2017). The three steps of AR1 dye molecule adsorption onto the adsorbent surface were verified by the multilinearity of the curves. Initially, the dye molecule entered the adsorbent's exterior surface through film diffusion. Subsequently, it slowly permeated the adsorbent's internal pores through intraparticle diffusion. The last step matched the stage for final equilibrium, and the second stage was more stable than the first, suggesting that it was the phase for determining out the rate (Al-Harby et al., 2021).

http://www.aloki.hu ● ISSN 1589 1623 (Print) ● ISSN 1785 0037 (Online)
DOI: http://dx.doi.org/10.15666/aeer/2402_24592501

Elovich model

Elovich model describes a chemisorption process where the adsorption energy decreases exponentially with increasing surface coverage. When adsorption involves a chemisorption process onto an adsorbent surface, this model takes place, and as time goes on, the adsorption speed reduces because the adsorbent surface is covered in an adsorbate (Guarín et al., 2018). It proposes a linear relationship between $\ln(q_t)$ and time (t) as presented in *Figure A5*. The values of constant related to the desorption constant (β), Initial adsorption rate (α) (mg/g/min), and the respective R^2 were summarized in *Table 8*. β = 1.594 g/mg**,** indicates a slow desorption rate, suggesting strong binding between dye molecules and adsorbent. While, the higher values of α = (6.3661×10^{26} mg/g/min) represent a faster initial adsorption rate, suggesting a stronger driving force for adsorption. The low R^2 value (0.0726) suggests a poor fit of the model to the experimental data, indicating that the chemisorption process might not be the dominant mechanism in this system. The poor fit suggests that the adsorption might not be purely a chemisorption process. The role of physisorption or other interaction mechanisms might be significant.

The analysis of the different kinetic models suggests that the pseudo second-order model best describes the adsorption of Acid Red 1 dye onto the AC-ZnO-NH_3 composite. This is supported by the high R^2 value and the agreement between the calculated and experimental Q_e values. The model indicates that the adsorption process might be dominated by chemical interactions between the dye molecules and the active sites on the composite, with a strong dependence on the availability of vacant sites. However, it is important to note that the other models (intraparticle diffusion and Elovich) may still play a role in the adsorption process, but their contribution might be less significant compared to the second-order mechanism.

Evaluation of reusability and regeneration

The regeneration experiments conducted to assess the reusability of the Multifunctional AC-ZnO-NH_3 Composite demonstrated significant initial adsorption efficiency but revealed a decline in performance over successive regeneration cycles. *Table 8* showed the removal efficiencies recorded were 88.571% for first stage, 37.778% for second stage and the third stage was 27.937%. The initial high removal efficiency highlights the composite's excellent adsorption capability during the first cycle. However, the sharp decrease in removal efficiency in subsequent cycles suggests the presence of irreversible adsorption sites, incomplete desorption, or structural/chemical degradation of the composite material during regeneration processes (Lashaki et al., 2012). Correspondingly, the sharp decline in removal efficiency after the first stage could be attributed to during the initial adsorption, strong chemisorption interactions may have occurred between the dye molecules and the active sites of the composite material, leading to incomplete regeneration. Residual dye molecules might block active adsorption sites, reducing available surface area and adsorption efficiency in subsequent cycles (Abualnaja et al., 2021b). Repeated exposure to dyes and regeneration chemicals might alter the surface chemistry of the composite, reducing its affinity for the dye molecules (Larasati et al., 2021).

Table 8. *Evaluation of regeneration of AC-ZnO-NH_3 composite*

Regeneration (NO)	% Removal
The first stage	88.571
The second stage	37.778
The third stage	27.937

http://www.aloki.hu ● ISSN 1589 1623 (Print) ● ISSN 1785 0037 (Online)
DOI: http://dx.doi.org/10.15666/aeer/2402_24592501

Suggested cost estimation

This study was designed to evaluate the feasibility of producing a multifunctional composite material, AC-ZnO-NH$_3$, and its application in removing dye contaminants from wastewater. The choice of this composite is based on its promising adsorptive and antimicrobial properties, making it a viable candidate for wastewater treatment. The methodology focused on minimizing costs while ensuring high performance, thus making the process suitable for large-scale applications (Alprol et al., 2025b). The research utilized locally available materials, simple preparation techniques, and optimized processing conditions through statistical modeling (Box-Behnken Design). This approach reduced experimental costs and ensured efficient removal of contaminants. The primary objective of this study is to provide a detailed and accurate cost estimation for producing 1 kg of AC-ZnO-NH$_3$ composite and its application in treating 1.5 cubic meters of wastewater contaminated with Acid Red 1 dye. The pricing in this study is based on the following factors: prices were derived from current market rates for chemicals and raw materials, including activated carbon, zinc oxide, and ammonia. Costs reflect small-scale laboratory purchases. Energy consumption was calculated based on the operating time and power ratings of equipment (e.g., magnetic stirrers, ovens, and furnaces). Average industrial electricity rates were used to estimate energy costs. Expenses reflect standard laboratory service charges for advanced analytical techniques like SEM, FTIR, and EDX, which are widely used in material characterization. Also, the energy and water costs were also factored into the calculations. Labor costs include wages for technical personnel, researchers, and supervisors. Charges for statistical modeling and design optimization (Box-Behnken Design) were also considered. The study emphasizes minimizing costs while maintaining high efficiency. It leverages locally available materials and simple preparation techniques, making the process scalable and cost-effective for larger applications. The data in *Table 9* showed that the AC-ZnO-NH$_3$ composite can be produced at a very low cost (less than $200 per kg). High removal efficiency of Acid Red 1 dye (up to 99.75%) under optimal conditions (pH 3, 50 mg/L dye concentration, 10 mg adsorbent, and 90 min contact time) (Alprol et al., 2025a).

Table 9. *Cost analysis of AC-ZnO-NH$_3$ composite production and its application in industrial wastewater treatment*

Item	Cost (USD)
1. Raw material costs	$4.65
Activated carbon	$1.75
Zinc oxide nanoparticles (ZnO)	$1.05
Ammonia solution	$0.35
Distilled water and additional chemicals	$1.50
2. Preparation and processing costs	$18.50
Magnetic stirring (30 min at 80–100°C)	$1.50
Drying (12 h at 100°C)	$4.00
Heating at 400°C for 1 h (thermal activation)	$6.00
Superheated steam activation	$7.00
3. Characterization and Analytical Costs	$55.00
Scanning electron microscopy (SEM)	$20.00
Fourier transform infrared spectroscopy (FTIR)	$20.00
Energy dispersive X-ray analysis (EDX)	$15.00

http://www.aloki.hu ● ISSN 1589 1623 (Print) ● ISSN 1785 0037 (Online)
DOI: http://dx.doi.org/10.15666/aeer/2402_24592501

Item	Cost (USD)
4. Operational Costs for Wastewater Treatment	$12.00
Required Dose (0.03 g per liter for 1.5 m^3 wastewater)	$12.00
5. Labor and supervision costs	$100.00
Technical and laboratory labor	$60.00
Supervision and statistical analysis (Box-Behnken design)	$40.00
6. Total estimated costs (low-cost plan)	$190.15

Conclusion

This study demonstrated the efficiency of the AC-ZnO-NH$_3$ nanocomposite for removing Acid Red 1 dye from aqueous solutions. The material showed a porous structure and high surface area, confirmed by SEM and EDX analyses, indicating the presence of activated carbon, ZnO, and FeO. FTIR analysis revealed multiple functional groups supporting adsorption through electrostatic attraction, hydrogen bonding, and π–π interactions. Optimization using the Box-Behnken Design identified pH, dye concentration, adsorbent dosage, and contact time as key parameters, achieving a maximum dye removal of 99.75% under optimal conditions. Kinetic studies followed the pseudo-second-order model, indicating chemical interactions between the dye and active sites, while the Langmuir isotherm best described equilibrium data, confirming monolayer adsorption with a capacity of 312.5 mg/g. Thermodynamic results suggested an endothermic, temperature-dependent adsorption process. The combined ZnO and ammonia modification significantly enhanced the composite's adsorption and antibacterial properties, offering dual functionality for both dye removal and microbial inhibition. Overall, AC-ZnO-NH$_3$ represents a robust, multifunctional, and sustainable adsorbent for effective wastewater treatment and decolorization applications.

Author contributions. Sameerah I. Al-Saeedi: Validation, Investigation, Software, Resources, Funding acquisition, Visualization, Writing—review and editing. **Mohamed Ashour:** Visualization, Software, Investigation, Validation, Resources, Writing—original draft preparation, Writing—review and editing. **Ahmed E. Alprol:** Conceptualization, Methodology, investigation, Software, Formal analysis, Writing—review and editing, Writing—original draft preparation, Project administration. **Ghadah M. Al-Senani:** Investigation, Software, Validation, Visualization, Writing—review and editing.

Funding. The authors express their gratitude to the support Deanship of Scientific Research, Vice Presidency for Graduate Studies and Scientific Research, King Faisal University, Saudi Arabia (KFU260182). This research project was funded by the Deanship of Scientific Research and Libraries, Princess Nourah bint Abdulrahman University, through the Program of Research Project Funding After Publication, grant No (RPFAP-102- 1445).

Conflict of interests. The authors declare no conflict of interest.

Data availability statement. The original contributions presented in this study are included in the article/supplementary material. Further inquiries can be directed to the corresponding author.

REFERENCES

[1] Abd El-Hamid, H. T., AlProl, A. E., Hafiz, M. A. (2022): The efficiency of adsorption modelling and Plackett-Burman design for remediation of crystal violet by *Sargassum latifolium*. – Biocatalysis and Agricultural Biotechnology 44: 102459. https://doi.org/10.1016/j.bcab.2022.102459.

http://www.aloki.hu ● ISSN 1589 1623 (Print) ● ISSN 1785 0037 (Online)
DOI: http://dx.doi.org/10.15666/aeer/2402_24592501

[2] Abdallah, M. A. M., Alprol, A. E. (2024a): Utilization of aquatic biomass as biosorbent for sustainable production of high surface area, nano- microporous, for removing two dyes from wastewater. – Scientific Reports 14(1): 4471. https://doi.org/10.1038/s41598-024-54539-2.

[3] Abdallah, M. A. M., Alprol, A. E. (2024b): Utilization of aquatic biomass as biosorbent for sustainable production of high surface area, nano- microporous, for removing two dyes from wastewater. – Scientific Reports 14(1): 4471. https://doi.org/10.1038/s41598-024-54539-2.

[4] Abualnaja, K. M., Alprol, A. E., Abu-Saied, M. A., Mansour, A. T., Ashour, M. (2021a): Studying the adsorptive behavior of poly(acrylonitrile-co-styrene) and carbon nanotubes (nanocomposites) impregnated with adsorbent materials towards methyl orange dye. – Nanomaterials 11(5): 1144. https://doi.org/10.3390/nano11051144.

[5] Abualnaja, K. M., Alprol, A. E., Ashour, M., Mansour, A. T. (2021b): Influencing multi-walled carbon nanotubes for the removal of ismate violet 2R dye from wastewater: isotherm, kinetics, and thermodynamic studies. – Appl. Sci. 11(11): 1-26. https://doi.org/10.3390/app11114786.

[6] Al Prol, A. E. (2019): Study of environmental concerns of dyes and recent textile effluents treatment technology: a review. – Asian Journal of Fisheries and Aquatic Research 3(2): 1-18. https://doi.org/10.9734/ajfar/2019/v3i230032.

[7] Al-Ajji, M. A., Al-Ghouti, M. A. (2021): Novel insights into the nanoadsorption mechanisms of crystal violet using nano-hazelnut shell from aqueous solution. – Journal of Water Process Engineering 44: 102354. https://doi.org/10.1016/j.jwpe.2021.102354.

[8] Al-Harby, N. F., Albahly, E. F., Mohamed, N. A. (2021): Kinetics, isotherm and thermodynamic studies for efficient adsorption of Congo red dye from aqueous solution onto novel cyanoguanidine-modified chitosan adsorbent. – Polymers 13(24): 4446. https://doi.org/10.3390/polym13244446.

[9] Alprol, A. E. (2024): The use of adsorption technology in the removal of dyes and heavy metals from aqueous solution by agricultural wastes. – Blue Economy 2: 1-10.

[10] Alprol, A. E., Mansour, A. T., Abdelwahab, A. M., Ashour, M. (2023): Advances in green synthesis of metal oxide nanoparticles by marine algae for wastewater treatment by adsorption and photocatalysis techniques. – Catalysts 13(5): 888. https://doi.org/10.3390/catal13050888.

[11] Alprol, A. E., Bakr, A., Al-Saeedi, S. I., Mansour, A. T., El-Haroun, E., Alharthi, M. N., Ashour, M. (2025a): Chitosan/ferrous oxide nanocomposite for the sunlight-driven photocatalytic degradation of organic azo dye in aqueous solutions and aquaculture effluents wastewater. – Scientific Reports 15(1): 23289. https://doi.org/10.1038/s41598-025-04207-w.

[12] Alprol, A. E., Manaa, A., Basaham, A. S., Ghandour, I. M., El-Regal, M. A. A., El-Metwally, M. E. A. (2025b): Optimized removal of methylene blue from wastewater using an activated carbon-zinc oxide-ammonia composite. – Scientific Reports 15(1): 38834. https://doi.org/10.1038/s41598-025-08783-9.

[13] Al-Saeedi, S. I., Ashour, M., Alprol, A. E. (2023): Adsorption of toxic dye using red seaweeds from synthetic aqueous solution and its application to industrial wastewater effluents. – Frontiers in Marine Science 10. https://doi.org/10.3389/fmars.2023.1202362.

[14] Al-Tohamy, R., Ali, S. S., Li, F., Okasha, K. M., Mahmoud, Y. A.-G., Elsamahy, T., Jiao, H., Fu, Y., Sun, J. (2022): A critical review on the treatment of dye-containing wastewater: ecotoxicological and health concerns of textile dyes and possible remediation approaches for environmental safety. – Ecotoxicology and Environmental Safety 231: 113160. https://doi.org/10.1016/j.ecoenv.2021.113160.

[15] Amrutha, Jeppu, G., Girish, C. R., Prabhu, B., Mayer, K. (2023): Multi-component adsorption isotherms: review and modeling studies. – Environmental Processes 10(2): 38. https://doi.org/10.1007/s40710-023-00631-0.

http://www.aloki.hu ● ISSN 1589 1623 (Print) ● ISSN 1785 0037 (Online)
DOI: http://dx.doi.org/10.15666/aeer/2402_24592501

[16] Anand, M., Suresh, S. (2015): Marine seaweed Sargassum wightii extract as a low-cost sensitizer for ZnO photoanode based dye-sensitized solar cell. – Advances in Natural Sciences: Nanoscience and Nanotechnology 6(3): 035008. https://doi.org/10.1088/2043-6262/6/3/035008.

[17] Awasthi, M. K., Amobonye, A., Bhagwat, P., Ashokkumar, V., Gowd, S. C., Dregulo, A. M., Rajendran, K., Flora, G., Kumar, V., Pillai, S., Zhang, Z., Sindhu, R., Taherzadeh, M. J. (2024): Biochemical engineering for elemental sulfur from flue gases through multi-enzymatic based approaches—a review. – Science of the Total Environment 914: 169857.

[18] Bailon-Ruiz, S. J., Cedeño-Mattei, Y., Torres-Torres, K., Alamo-Nole, L. (2023): Photodegradation of tropaeolin O in the presence of Ag-doped ZnO nanoparticles. – Micro 3(3): 643-652. https://doi.org/10.3390/micro3030045.

[19] Beg, S., Akhter, S. (2021): Box–Behnken Designs and Their Applications in Pharmaceutical Product Development. – In: Beg. S. (ed.) Design of Experiments for Pharmaceutical Product Development. Springer, Singapore, pp. 77-85. https://doi.org/10.1007/978-981-33-4717-5_7.

[20] Beig, B., Niazi, M. B. K., Jahan, Z., Haider, G., Zia, M., Shah, G. A., Iqbal, Z., Hayat, A. (2023): Development and testing of zinc sulfate and zinc oxide nanoparticle-coated urea fertilizer to improve N and Zn use efficiency. – Frontiers in Plant Science 13. https://doi.org/10.3389/fpls.2022.1058219.

[21] Bullen, J. C., Saleesongsom, S., Gallagher, K., Weiss, D. J. (2021): A revised pseudo-second-order kinetic model for adsorption, sensitive to changes in adsorbate and adsorbent concentrations. – Langmuir 37(10): 3189-3201. https://doi.org/10.1021/acs.langmuir.1c00142.

[22] Das, P., Sa, J.-H., Kim, K.-H., Jeon, E.-C. (2009): Effect of fertilizer application on ammonia emission and concentration levels of ammonium, nitrate, and nitrite ions in a rice field. – Environmental Monitoring and Assessment 154(1-4): 275-282. https://doi.org/10.1007/s10661-008-0395-2.

[23] Das, S., Mishra, S. (2017): Box-Behnken statistical design to optimize preparation of activated carbon from Limonia acidissima shell with desirability approach. – Journal of Environmental Chemical Engineering 5(1): 588-600. https://doi.org/10.1016/j.jece.2016.12.034.

[24] de Franco, M. A. E., de Carvalho, C. B., Bonetto, M. M., de Pelegrini Soares, R., Féris, L. A. (2018): Diclofenac removal from water by adsorption using activated carbon in batch mode and fixed-bed column: isotherms, thermodynamic study and breakthrough curves modeling. – Journal of Cleaner Production 181: 145-154. https://doi.org/10.1016/j.jclepro.2018.01.138.

[25] DeChant, C. M., Moradkhani, H. (2014): Toward a reliable prediction of seasonal forecast uncertainty: addressing model and initial condition uncertainty with ensemble data assimilation and sequential Bayesian combination. – Journal of Hydrology 519: 2967-2977. https://doi.org/10.1016/j.jhydrol.2014.05.045.

[26] Deniz, F., Saygideger, S. D. (2011): Removal of a hazardous azo dye (Basic Red 46) from aqueous solution by princess tree leaf. – Desalination 268(1-3): 6-11. https://doi.org/10.1016/j.desal.2010.09.043.

[27] Dubey, R., Bajpai, J., Bajpai, A. K. (2015): Green synthesis of graphene sand composite (GSC) as novel adsorbent for efficient removal of Cr (VI) ions from aqueous solution. – Journal of Water Process Engineering 5: 83-94. https://doi.org/10.1016/j.jwpe.2015.01.004.

[28] Elzahar, M. M. H., Bassyouni, M. (2023): Removal of direct dyes from wastewater using chitosan and polyacrylamide blends. – Scientific Reports 13(1): 15750. https://doi.org/10.1038/s41598-023-42960-y.

[29] Fernandes, J. V., Rodrigues, A. M., Menezes, R. R., Neves, G. de A. (2020): Adsorption of anionic dye on the acid-functionalized bentonite. – Materials 13(16): 3600.

http://www.aloki.hu ● ISSN 1589 1623 (Print) ● ISSN 1785 0037 (Online)
DOI: http://dx.doi.org/10.15666/aeer/2402_24592501

https://doi.org/10.3390/ma13163600.

[30] Fonseca, J. M., Spessato, L., Cazetta, A. L., da Silva, C., Almeida, V. de C. (2022): Sulfonated carbon: synthesis, properties and production of biodiesel. – Chemical Engineering and Processing—Process Intensification 170: 108668. https://doi.org/10.1016/j.cep.2021.108668.

[31] Freundlich, H. (1906): Über die Adsorption in Lösungen. – Habilitationsschrift durch welche... zu haltenden Probevorlesung "Kapillarchemie und Physiologie" einladet Dr. Herbert Freundlich. – W. Engelmann, Leipzig.

[32] Gottipati, R., Mishra, S. (2010): Process optimization of adsorption of Cr(VI) on activated carbons prepared from plant precursors by a two-level full factorial design. – Chemical Engineering Journal 160(1): 99-107. https://doi.org/10.1016/j.cej.2010.03.015.

[33] Goulet-Pelletier, J.-C., Cousineau, D. (2018): A review of effect sizes and their confidence intervals, Part I: The Cohen's d family. – The Quantitative Methods for Psychology 14(4): 242-265. https://doi.org/10.20982/tqmp.14.4.p242.

[34] Guarín, J. R., Moreno-Pirajan, J. C., Giraldo, L. (2018): kinetic study of the bioadsorption of methylene blue on the surface of the biomass obtained from the algae D. antarctica. – Journal of Chemistry 2018: 1-12. https://doi.org/10.1155/2018/2124845.

[35] Harkins, W. D., Jura, G. (1944): Surfaces of solids. XIII. A vapor adsorption method for the determination of the area of a solid without the assumption of a molecular area, and the areas occupied by nitrogen and other molecules on the surface of a solid. – Journal of the American Chemical Society 66(8): 1366-1373. https://doi.org/10.1021/ja01236a048. https://doi.org/10.1016/j.scitotenv.2023.169857.

[36] Imla Syafiqah, M. S., Yussof, H. W. (2018): Kinetics, isotherms, and thermodynamic studies on the adsorption of mercury (ii) ion from aqueous solution using modified palm oil fuel ash. – Materials Today: Proceedings 5(10): 21690-21697. https://doi.org/10.1016/j.matpr.2018.07.020.

[37] Jain, D., Pareek, S., Chattopadhyay, S., Behera, D. (2020): Ni-doped ZnO-chitin composites for anti-corrosive coating on Zn alloy in simulated body fluid solution. – Journal of Bio- and Tribo-Corrosion 6(4): 113. https://doi.org/10.1007/s40735-020-00411-5.

[38] Jayan, N., Bhatlu. M. L. D., Akbar, S. T. (2021) :Central composite design for adsorption of Pb(II) and Zn(II) metals on PKM-2 Moringa oleifera leaves. – ACS Omega 6(39): 25277-25298. https://doi.org/10.1021/acsomega.1c03069.

[39] Joshi, S., Shrestha, R. G., Pradhananga, R. R., Ariga, K., Shrestha, L. K. (2021): High surface area nanoporous activated carbons materials from areca catechu nut with excellent iodine and methylene blue adsorption. – C 8(1): 2. https://doi.org/10.3390/c8010002.

[40] Kadam, A. A., Sharma, B., Shinde, S. K., Ghodake, G. S., Saratale, G. D., Saratale, R. G., Kim, D.-Y., Sung, J.-S. (2020): Thiolation of chitosan loaded over super-magnetic halloysite nanotubes for enhanced laccase immobilization. – Nanomaterials 10(12): 2560. https://doi.org/10.3390/nano10122560.

[41] Khamkeaw, A., Asavamongkolkul, T., Perngyai, T., Jongsomjit, B., Phisalaphong, M. (2020): Interconnected micro, meso, and macro porous activated carbon from bacterial nanocellulose for superior adsorption properties and effective catalytic performance. – Molecules 25(18): 4063. https://doi.org/10.3390/molecules25184063.

[42] Langmuir, I. (1917): The constitution and fundamental properties of solids and liquids. – Journal of the Franklin Institute 183(1): 102-105. https://doi.org/10.1016/S0016-0032(17)90938-X.

[43] Larasati, A., Fowler, G. D., Graham, N. J. D. (2021): Insights into chemical regeneration of activated carbon for water treatment. – Journal of Environmental Chemical Engineering 9(4): 105555. https://doi.org/10.1016/j.jece.2021.105555.

http://www.aloki.hu ● ISSN 1589 1623 (Print) ● ISSN 1785 0037 (Online)
DOI: http://dx.doi.org/10.15666/aeer/2402_24592501

[44] Lashaki, M. J., Fayaz, M., Wang, H., Hashisho, Z., Philips, J. H., Anderson, J. E., Nichols, M. (2012): Effect of adsorption and regeneration temperature on irreversible adsorption of organic vapors on beaded activated carbon. – Environmental Science & Technology 46(7): 4083-4090. https://doi.org/10.1021/es3000195.
[45] Lin, C., Li, S., Chen, M., Jiang, R. (2017): Removal of Congo red dye by gemini surfactant C 12 -4-C 12 · 2Br-modified chitosan hydrogel beads. – Journal of Dispersion Science and Technology 38(1): 46-57. https://doi.org/10.1080/01932691.2016.1138229.
[46] Lund, P., Tramonti, A., De Biase, D. (2014): Coping with low pH: molecular strategies in neutralophilic bacteria. – FEMS Microbiology Reviews 38(6): 1091-1125. https://doi.org/10.1111/1574-6976.12076.
[47] Manisalidis, I., Stavropoulou, E., Stavropoulos, A., Bezirtzoglou, E. (2020): Environmental and health impacts of air pollution: a review. – Frontiers in Public Health 8. https://doi.org/10.3389/fpubh.2020.00014.
[48] Mansour, A. T., Alprol, A. E., Khedawy, M., Abualnaja, K. M., Shalaby, T. A., Rayan, G., Ramadan, K. M. A., Ashour, M. (2022): Green synthesis of zinc oxide nanoparticles using red seaweed for the elimination of organic toxic dye from an aqueous solution. – Materials 15(5169): 1-25. https://doi.org/10.3390/ma15155169.
[49] Marchessault, R. H., Pearson, F. G., Liang, C. Y. (1960): Infrared spectra of crystalline polysaccharides. – Biochimica et Biophysica Acta 45: 499-507. https://doi.org/10.1016/0006-3002(60)91486-4.
[50] Mustapha, S., Shuaib, D. T., Ndamitso, M. M., Etsuyankpa, M. B., Sumaila, A., Mohammed, U. M., Nasirudeen, M. B. (2019): Adsorption isotherm, kinetic and thermodynamic studies for the removal of Pb(II), Cd(II), Zn(II) and Cu(II) ions from aqueous solutions using Albizia lebbeck pods. – Applied Water Science 9(6): 142. https://doi.org/10.1007/s13201-019-1021-x.
[51] Nannu Shankar, S., Dinakaran, D. R., Chandran, D. K., Mantha, G., Srinivasan, B., Nyayiru Kannaian, U. P. (2023): Adsorption kinetics, equilibrium and thermodynamics of a textile dye V5BN by a natural nanocomplex material: clinoptilolite. – Energy Nexus 10: 100197. https://doi.org/10.1016/j.nexus.2023.100197.
[52] Nath, H., Das, J., Debnath, C., Sarkar, B., Saxena, R., Barma, S. D. (2023): Development of lignocellulosic biomass derived Cu and Zn doped highly porous activated carbon and its utilization in the anti-microbial treatment. – Environmental Chemistry and Ecotoxicology 5: 155-164. https://doi.org/10.1016/j.enceco.2023.07.001.
[53] Pelekani, C., Snoeyink, V. L. (2001): A kinetic and equilibrium study of competitive adsorption between atrazine and Congo red dye on activated carbon: the importance of pore size distribution. – Carbon 39(1): 25-37. https://doi.org/10.1016/S0008-6223(00)00078-6.
[54] Ramaprabha, K., Kumar, S. V. (2025): Effective photocatalytic degradation and kinetic modelling of azo dyes by zinc oxide nanoparticles from Brevibacterium casei. – Desalination and Water Treatment 321: 100936. https://doi.org/10.1016/j.dwt.2024.100936.
[55] Rezazadeh, M., Baghdadi, M., Mehrdadi, N., Ali Abdoli, M. (2020): Adsorption of crystal violet dye by agricultural rice bran waste: isotherms, kinetics, modeling and influencing factors. – Environmental Engineering Research. https://doi.org/10.4491/eer.2020.128.
[56] Sahu, N., Nayak, A. K., Verma, L., Bhan, C., Singh, J., Chaudhary, P., Yadav, B. C. (2022): Adsorption of As(III) and As(V) from aqueous solution by magnetic biosorbents derived from chemical carbonization of pea peel waste biomass: isotherm, kinetic, thermodynamic and breakthrough curve modeling studies. – Journal of Environmental Management 312: 114948. https://doi.org/10.1016/j.jenvman.2022.114948.
[57] Samimi, M., Shahriari-Moghadam, M. (2023): The Lantana camara L. – stem biomass as an inexpensive and efficient biosorbent for the adsorptive removal of malachite green from aquatic environments: kinetics, equilibrium and thermodynamic studies. International Journal of Phytoremediation 25(10): 1328-1336. https://doi.org/10.1080/15226514.2022.2156978.

http://www.aloki.hu ● ISSN 1589 1623 (Print) ● ISSN 1785 0037 (Online)
DOI: http://dx.doi.org/10.15666/aeer/2402_24592501

[58] Shaheen, R., Hanif, M. A. (2024): Revolutionizing dye removal from wastewater using low-cost natural material. – Desalination and Water Treatment 319: 100580. https://doi.org/10.1016/j.dwt.2024.100580.
[59] Sharma, G., Sharma, S., Kumar, A., Lai, C. W., Naushad, Mu., Shehnaz, Iqbal, J., Stadler, F. J. (2022): Activated carbon as superadsorbent and sustainable material for diverse applications. – Adsorption Science & Technology. https://doi.org/10.1155/2022/4184809.
[60] Sulaiman, N. S., Mohamad Amini, M. H., Danish, M., Sulaiman, O., Hashim, R. (2021): Kinetics, thermodynamics, and isotherms of methylene blue adsorption study onto cassava stem activated carbon. – Water 13(20): 2936. https://doi.org/10.3390/w13202936.
[61] Tempkin, M. J., Pyzhev, V. (1940): Kinetics of ammonia synthesis on promoted iron catalysts. – Acta Physiochim, URSS (Vol. 12).
[62] Thomas, S., Sreekanth, R., Sijumon, V. A., Aravind, U. K., Aravindakumar, C. T. (2014): Oxidative degradation of Acid Red 1 in aqueous medium. – Chemical Engineering Journal 244: 473-482. https://doi.org/10.1016/j.cej.2014.01.037.
[63] Uddin, M. K., Rao, R. A. K., Chandra Mouli, K. V. V. (2018): The artificial neural network and Box-Behnken design for Cu2 + removal by the pottery sludge from water samples: equilibrium, kinetic and thermodynamic studies. – Journal of Molecular Liquids 266: 617-627. https://doi.org/10.1016/j.molliq.2018.06.098.
[64] Usman, M. O., Aturagaba, G., Ntale, M., Nyakairu, G. W. (2022): A review of adsorption techniques for removal of phosphates from wastewater. – Water Science and Technology 86(12): 3113-3132. https://doi.org/10.2166/wst.2022.382.
[65] Vaez, M., Zarringhalam Moghaddam, A., Alijani, S. (2012): Optimization and modeling of photocatalytic degradation of azo dye using a response surface methodology (RSM) based on the central composite design with immobilized titania nanoparticles. – Industrial & Engineering Chemistry Research 51(11): 4199-4207. https://doi.org/10.1021/ie202809w.
[66] Varala, S., Dharanija, B., Satyavathi, B., Basava Rao, V. V., Parthasarathy, R. (2016): New biosorbent based on deoiled Karanja seed cake in biosorption studies of Zr(IV): Optimization using Box–Behnken method in response surface methodology with desirability approach. – Chemical Engineering Journal 302: 786-800. https://doi.org/10.1016/j.cej.2016.05.088.
[67] Vázquez-Vélez, E., Martínez, H., Castillo, F. (2021): Degradation of Acid Red 1 catalyzed by peroxidase activity of iron oxide nanoparticles and detected by SERS. – Nanomaterials 11(11): 3044. https://doi.org/10.3390/nano11113044.
[68] Wu, R., Suhaimi, A., Jawad, A. H., ALOthman, Z. A. (2024): Decoration of chitosan-benzaldehyde/algae/coal fly ash adsorbent for brilliant green dye removal: Box–Benken design optimization and mechanism approach. – Journal of Inorganic and Organometallic Polymers and Materials 34(12): 5884-5900. https://doi.org/10.1007/s10904-024-03254-6.
[69] Zhu, H., Fu, Y., Jiang, R., Yao, J., Xiao, L., Zeng, G. (2014): Optimization of copper(II) adsorption onto novel magnetic calcium alginate/maghemite hydrogel beads using response surface methodology. – Industrial & Engineering Chemistry Research 53(10): 4059-4066. https://doi.org/10.1021/ie4031677.
[70] Zikalala, N. E., Azizi, S., Zikalala, S. A., Kamika, I., Maaza, M., Zinatizadeh, A. A., Mokrani, T., Kaviyarasu, K. (2022): An evaluation of the biocatalyst for the synthesis and application of zinc oxide nanoparticles for water remediation—a review. – Catalysts 12(11): 1442. https://doi.org/10.3390/catal12111442.

http://www.aloki.hu ● ISSN 1589 1623 (Print) ● ISSN 1785 0037 (Online)
DOI: http://dx.doi.org/10.15666/aeer/2402_24592501

APPENDIX

Table A1. *Examination of isotherm models*

Model	Equation	Plot
Langmuir	$\frac{q_e}{C_e} = K_a Q_m - K_a q_e$	q_e/C_e vs. q_e
	where: C_e is the equilibrium concentration of dye ion (mg/L), and Ka is the Langmuir constant (L/mg)	
Freundlich	$\log q_e = \log K_F + \frac{1}{n}\log C_e$	$\ln q_e$ vs. $\ln C_e$
	where: the intercept, log K_F, is a measure of adsorbent capacity, and the slope 1/n is the sorption intensity	
Tempkin	$\mathbf{q}_e = B \ln A + B \ln C_e$	q_e vs. lnCe
	where: A_T (L/g) are the Tempkin constant and B_T = (RT)/b while, T is the absoute temperature in Kelvin and R is the universal gas constant, 8.314 J/mol K. The constant b is related to the heat of adsorption	
Harkins–Jura	$\frac{1}{q_e^2} = (\frac{B_2}{A}) - (\frac{1}{A})\log C_e$	$1/qe^2$ vs. log Ce
	where: A (g^2/L) and B (mg^2/L) is two parameters characterizing the sorption equilibrium	

Table A2. *Adsorption kinetic models*

Model	Equation	Equation	Plot
Pseudo-first-order kinetic	$\text{Log}\ (q_e - q_t) = \log q_e - K_1 t / 2.303$	q_t (mg/g) is the amount of adsorbed AR1 on the sorbent at time t and k_1 (1/min) is the rate constant of first order sorption	A straight line of log ($q_e - q_t$) vs. t obtained with experimental data determined from the intercept and slope of the plot, respectively
Pseudo-second-order	$t/q_t = 1/k_2 q_e^2 + t/q_e$	K_2 (g/mg/min) is the rate constant of second-order sorption and can be rearranged and linearized to obtain	If second-order kinetics were applicable, the plot of t/q_t vs. t of experimental data should provide a straight line, and q_e and K_2 may be deduced from the slope and intercept of the plot, respectively
Intraparticle diffusion	$q_t = K_{dif} t^{1/2} + C$	K_{dif} (mg/g/min) is the intraparticle diffusion rate constant and C (mg/g) is related to the thickness of the boundary layer	K_{dif} and C values are calculated from the slope and intercept of q_t versus $t^{1/2}$ plots, respectively
Elovich	$Q_t = \frac{1}{\beta}\ln(\beta\alpha) + \frac{1}{\beta}\ln(t)$	The values of constant related to the desorption constant (β), Initial adsorption rate (α) (mg/g/min)	It proposes a linear relationship between $\ln(q_t)$ and time (t)

http://www.aloki.hu ● ISSN 1589 1623 (Print) ● ISSN 1785 0037 (Online)
DOI: http://dx.doi.org/10.15666/aeer/2402_24592501

Table A3. *ANOVA for linear model*

Source	Sum of squares	df	Mean square	F-value	p-Value	
Model	7482.94	4	1870.73	3.32	0.026	Significant
A-A	5422.18	1	5422.18	9.61	0.004	
B-B	397.65	1	397.65	0.704	0.409	
C-C	1100.09	1	1100.09	1.95	0.175	
D-D	563.01	1	563.01	0.998	0.327	
Residual	13538.02	24	564.08			
Lack of fit	11511.67	20	575.58	1.14	0.506	Not significant
Pure error	2026.35	4	506.59			
Cor total	21020.96	28				

Factor coding is Coded
Sum of squares is Type III – Partial
Response 1: R1

Table A4. *Coefficients in terms of coded factors and fit statistics*

Factor	Coefficient estimate	df	Standard error	95% CI low	95% CI high	VIF
Intercept	61.26	1	4.41	52.16	70.37	
A-A	-21.26	1	6.86	-35.41	-7.11	1.00
B-B	5.76	1	6.86	-8.39	19.91	1.00
C-C	9.57	1	6.86	-4.58	23.73	1.00
D-D	6.85	1	6.86	-7.30	21.00	1.00
R^2	0.3560					
Adjusted R^2	0.2486					
Predicted R^2	0.0433					
Adeq precision	6.2527					
Std. dev.	23.75					
Mean	61.26					
C.V. %	38.77					

http://www.aloki.hu ● ISSN 1589 1623 (Print) ● ISSN 1785 0037 (Online)
DOI: http://dx.doi.org/10.15666/aeer/2402_24592501

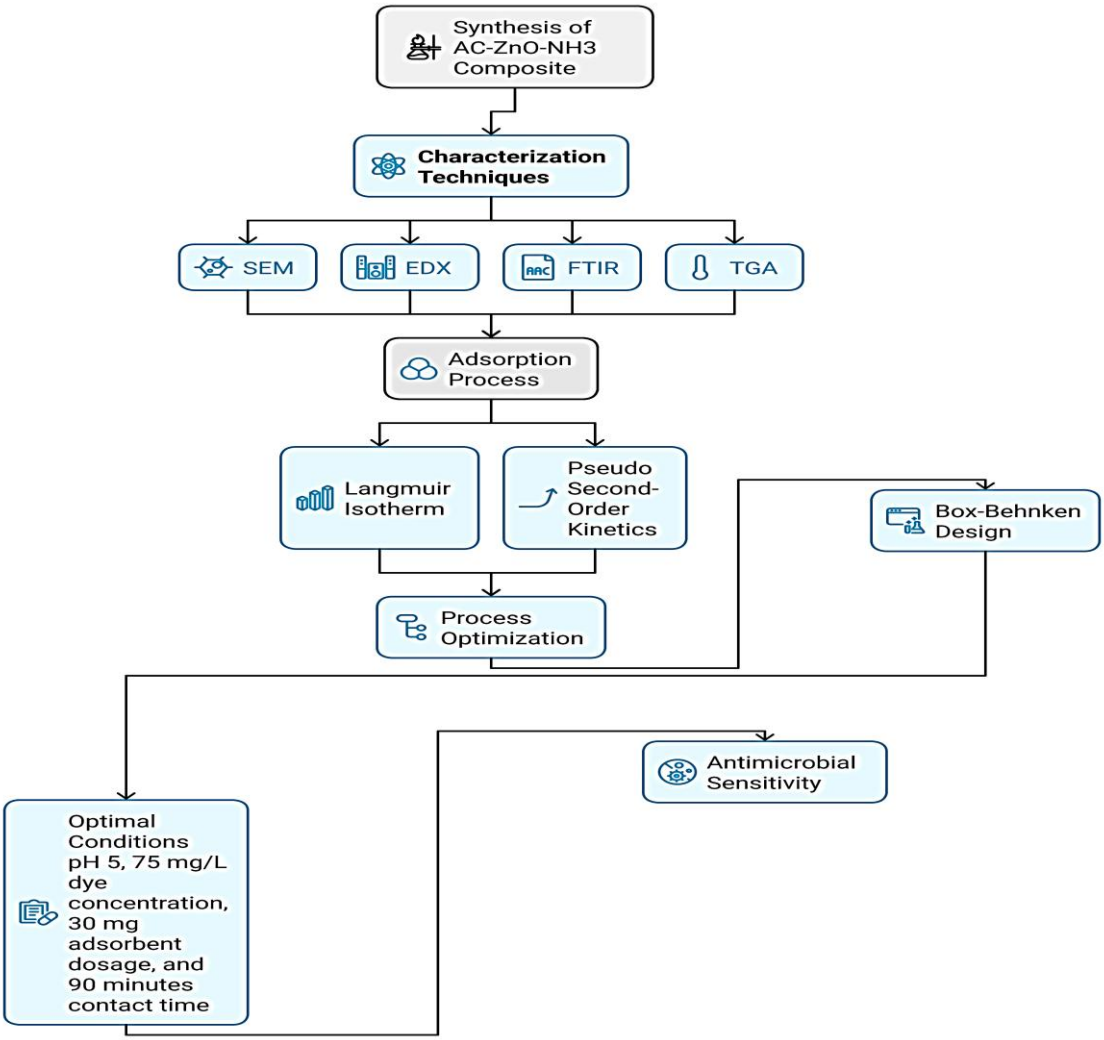

Figure A1. *The potential of AC-ZnO-NH₃ nanocomposite for the removal of Acid Red 1 dye from aqueous solutions using a BBD approach*

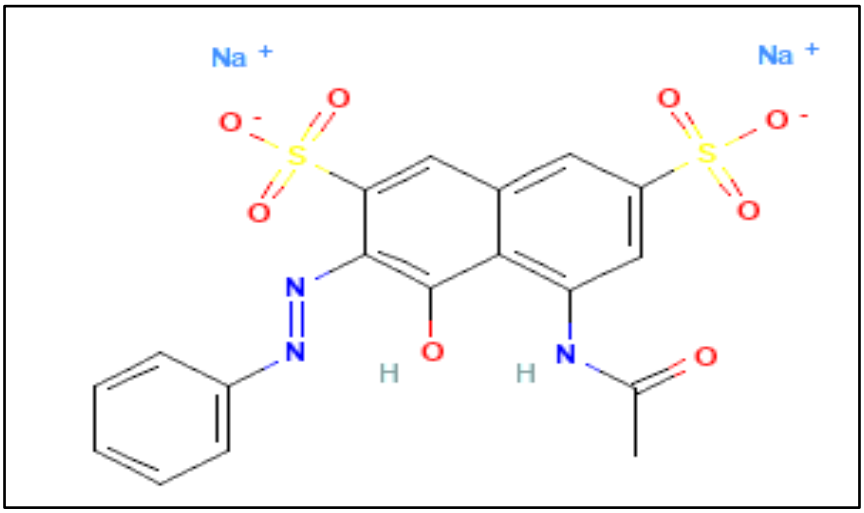

Figure A2. *Chemical structure of Acid Red 1 dye*

http://www.aloki.hu ● ISSN 1589 1623 (Print) ● ISSN 1785 0037 (Online)
DOI: http://dx.doi.org/10.15666/aeer/2402_24592501

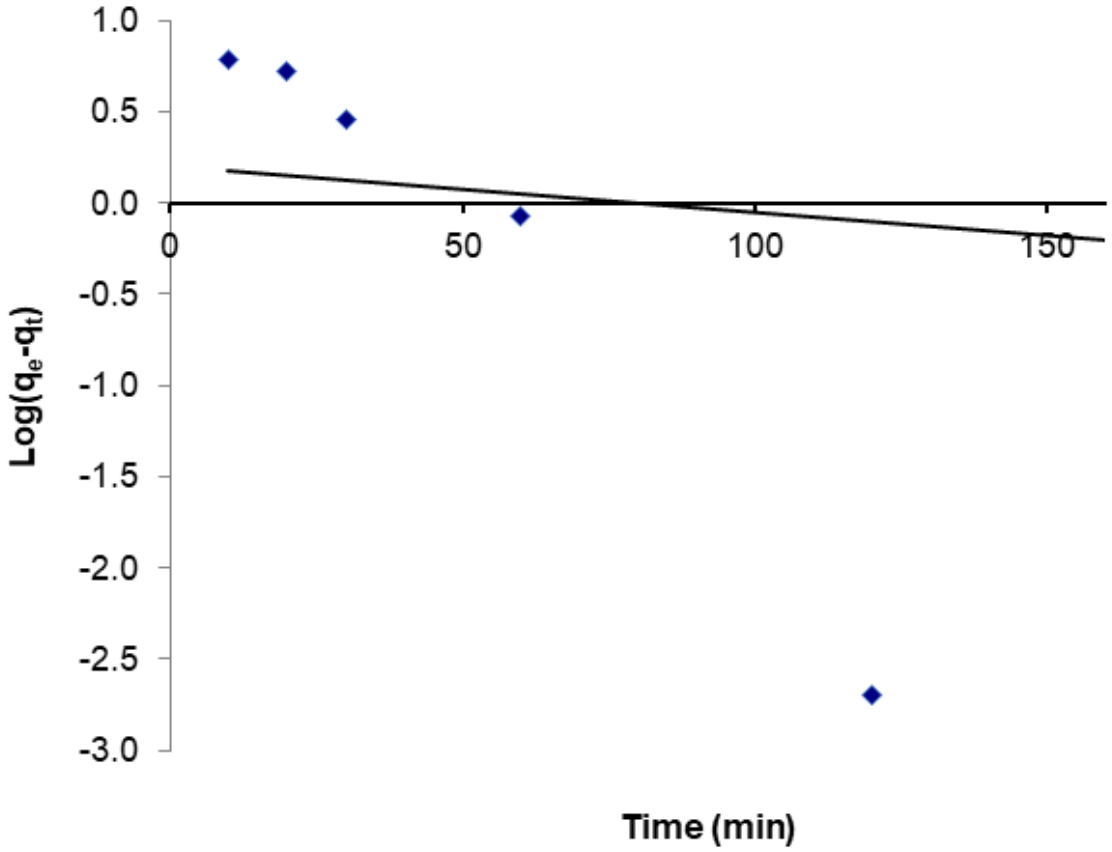

Figure A3. *Lagergren first-order kinetic model of AC-ZnO-NH3 nanocomposite for the removal of Acid Red 1 dye from aqueous solutions*

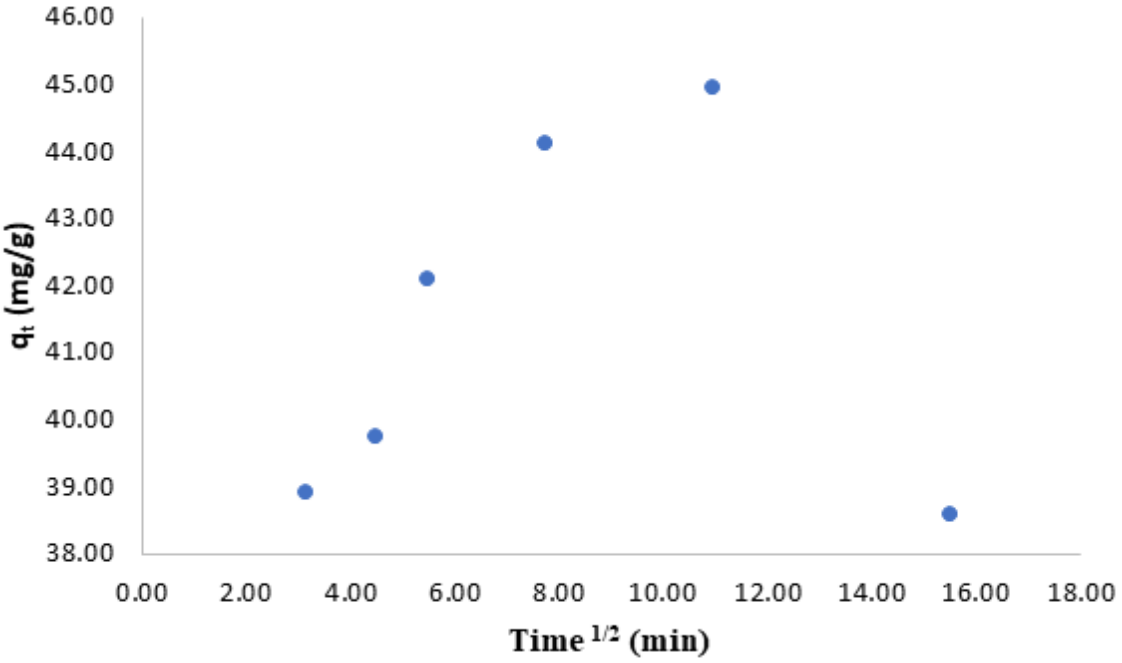

Figure A4. *Intraparticle diffusion model of AC-ZnO-NH₃ nanocomposite for the removal of Acid Red 1 dye from aqueous solutions*

http://www.aloki.hu ● ISSN 1589 1623 (Print) ● ISSN 1785 0037 (Online)
DOI: http://dx.doi.org/10.15666/aeer/2402_24592501

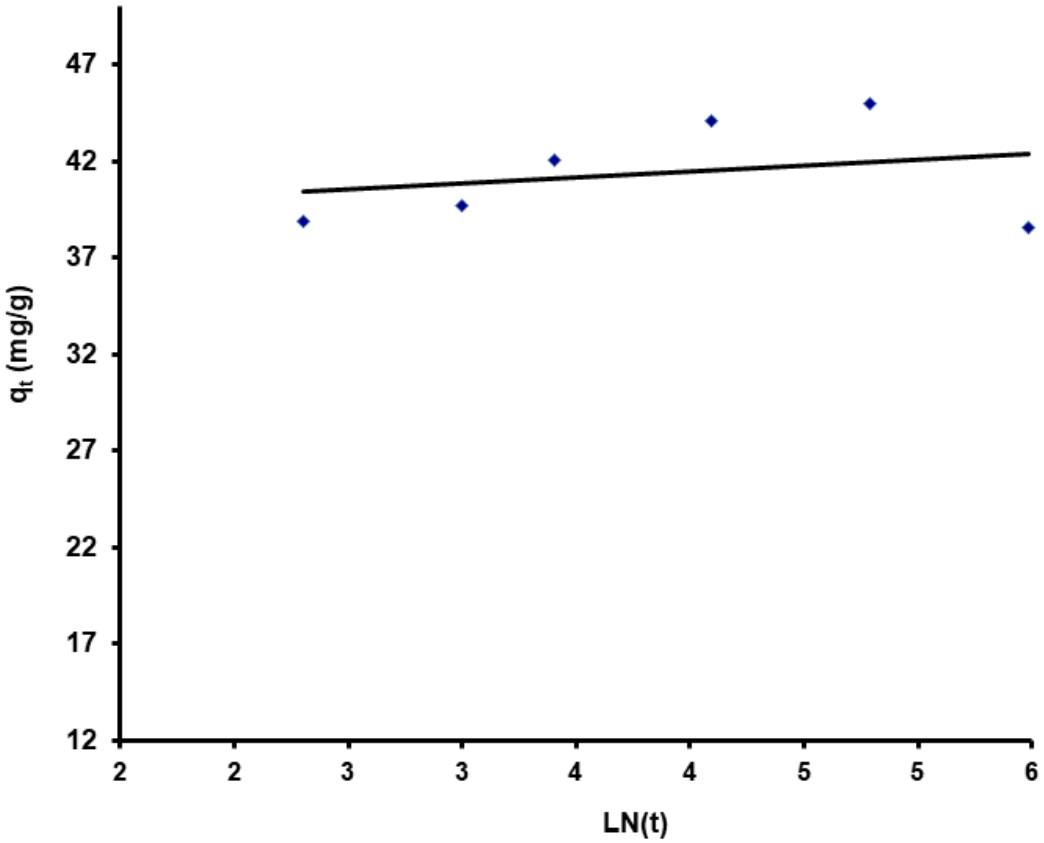

Figure A5. *Elovich kinetic model of AC-ZnO-NH3 nanocomposite for the removal of Acid Red 1 dye from aqueous solutions*

http://www.aloki.hu ● ISSN 1589 1623 (Print) ● ISSN 1785 0037 (Online)
DOI: http://dx.doi.org/10.15666/aeer/2402_24592501